

Electronic Thesis and Dissertation Repository

September 2020

Optimizing Preprocessing of fMRI Data to Maximize Correspondence of Functional Anatomy Across Individuals

Nargess Ghazaleh, *The University of Western Ontario*

Supervisor: Johnsrude, Ingrid, *The University of Western Ontario*

A thesis submitted in partial fulfillment of the requirements for the Master of Science degree in Neuroscience

© Nargess Ghazaleh 2020

Follow this and additional works at: <https://ir.lib.uwo.ca/etd>



Part of the [Cognitive Neuroscience Commons](#), [Computational Neuroscience Commons](#), and the [Diagnosis Commons](#)

Recommended Citation

Ghazaleh, Nargess, "Optimizing Preprocessing of fMRI Data to Maximize Correspondence of Functional Anatomy Across Individuals" (2020). *Electronic Thesis and Dissertation Repository*. 7286.
<https://ir.lib.uwo.ca/etd/7286>

This Dissertation/Thesis is brought to you for free and open access by Scholarship@Western. It has been accepted for inclusion in Electronic Thesis and Dissertation Repository by an authorized administrator of Scholarship@Western. For more information, please contact wlsadmin@uwo.ca.

Abstract

In movie-activation fMRI, intersubject correlation (ISC) indicates a functional correspondence across viewers. Brains differ in shape; spatial normalization and smoothing enhance inter-subject functional overlap. We compare three normalization methods and six smoothing levels to discover which method yields the best functional overlap, indexed by ISC. This is key to optimizing data analysis in clinical studies using movie-activation fMRI in future. In a 3T scanner, 44 healthy subjects watched an 8-min movie. Both normalization and smoothing affected the strength and extent of the ISC. ISC values were more robust for ANTs and DARTEL than for SPM12 and were (asymptotically) the strongest at 12mm smoothing. When image data are preprocessed with high-dimensional volumetric spatial registration methods, such as ANTs, and 12mm smoothing, the sensitivity of the movie-fMRI paradigm will be optimal for detecting abnormalities in presurgical evaluation of neurological patients, providing less variable and more reliable ISC measures.

Keywords: fMRI, Naturalistic Stimulation, Intersubject Correlation, Spatial Smoothing, Spatial Registration, Normalization

Summary for lay audience

Almost two in every 1000 of the world population has a neurologic disorder that requires brain surgery. Effective surgical treatment requires that the lesion be localized precisely, and resection does not result in unexpected cognitive decline. It is usually accomplished through preoperative assessment of patients using implanted electrodes or functional MRI (fMRI).

Current methods are not very sensitive to abnormalities in cognitive function. We propose to use fMRI to rapidly and noninvasively identify and map brain function. When neurologically healthy individuals watch an engaging film while undergoing fMRI (movie-driven fMRI), reliable and distinctive time-locked fluctuations in fMRI signals are observed throughout the brain. These fluctuations are different in different brain regions, reflecting the perceptual and cognitive demands of the film, but are very similar across people without neurological disorders (controls). The degree to which a patient's data matches predictions derived from control data can be tested statistically, region by region, to reveal functionally important cortex and local abnormalities of brain function. Because different brains differ in shape and size they should be registered to a standard template for comparison. The way the patient's data is registered to the template affects the sensitivity of the method to abnormalities.

We asked people without any neurological disorder to watch a short, suspenseful movie while they underwent a functional brain scan. We - for the first time - evaluated three different ways to register the movie-driven fMRI data. We found that the registration method that uses more points in data to match it with the template was more sensitive to fluctuations of the fMRI signal and as a result more sensitive to abnormalities. We also compiled this data set as a normative pattern of activity in a neurologically healthy population.

Movie-driven fMRI and this method of registration may be a valuable adjunct assessment method in the presurgical evaluation of neurologic patients. Future studies can compare the fMRI data from any individual patient with a neurologic disorder, such as focal epilepsy, with this normative pattern of brain signal fluctuation.

Acknowledgments

I would like to express my sincere gratitude to my supervisor Dr. Ingrid Johnsrude, for her scientific insight and mentoring, and for her guidance in encountering the unusual set of challenges encountered during my thesis. I am honored for having this privilege to work under her supervision.

I also want to thank my advisory committee members, Dr. Seyed Mirsattari, Dr. Brian Corneil, and Dr. Ali Khan, for their thoughtful comments and supports.

I also want to thank the current and past members of the CONCH lab (Cognitive Neuroscience of Communication and Hearing) group. Special thanks to Dr. Daniella Ladowski, whose guidance and friendship were a valuable asset to this work.

I am thankful to the clinical and research staff at University Hospital, London Health Sciences Centre, and the Imaging Centre of the Robarts Research Institute, London, ON. Pursuing this project was not possible without the help and support of Ms. Suzan Brown (research coordinator).

I acknowledge the help of Mr. Haitao Yang (IT manager of the Brain and Mind Institute) for his technical support during these years. His dedication to work is extremely admirable. Also, I am thankful to all the participants who volunteered their time for this project.

I also want to sincerely thank my parents Akram and Hojat, who always encourage me and are patient with my curiosities; my sisters Noushin and Naghmeh for their countless emotional and scientific support. Lastly, I want to express my deepest gratitude for my husband Ehsan, whose unconditional love and companionship are pivotal in pursuing my education.

To Bardiya

List of Abbreviations

ANTs	Advanced Normalization Tools
BOLD	Blood Oxygen Level Dependent
CSF	Cerebrospinal Fluid
DARTEL	The Diffeomorphic Anatomical Registration Through Exponentiated Lie Algebra
DRE	Drug Resistant Epilepsy
DTI	Diffusion Tensor Images
EEG	Electroencephalogram
FLAIR	Fluid Attenuation Inversion Recovery
FA	Flip Angle
fMRI	functional Magnetic Resonance Imaging
FWHM	Full Width at Half Maximum
GLM	General Linear Model
GM	Gray Matter
GRAPPA	Generalized Autocalibrating Partial Parallel
GRE	Gradient Echo
ICBM	International Consortium of Brain Mapping
iEEG	Intracranial Electroencephalogram
ISC	Inter-subject Correlation
MEG	Magnetoencephalography
MNI	Montreal Neurological Institute
PAT	Parallel Acquisition Techniques
PET	Positron Emission Tomography
RFT	Random Field Theory
rs-fMRI	resting state functional Magnetic Resonance Imaging
SPECT	Single Photon Emission Computerized Tomography
SPM	Statistical Parametric Mapping
TE	Echo time
TR	Repetition time
UWO	University of Western Ontario
WM	White Matter

Contents

Abstract	ii
Summary for lay audience	iii
Acknowledgements	iv
Dedication	v
List of Abbreviations	vi
List of Figures	ix
List of Tables	xi
List of Appendices	xii
1 Introduction	1
1.1 Presurgical assessment in Epilepsy	1
1.2 Functional Magnetic Resonance Imaging	2
1.2.1 Movie-fMRI	3
1.3 Inter-subject correlation basics	3
1.4 “Bang You’re Dead!”	4
1.5 Anatomical variability and processing of the fMRI data	5
1.6 Normalization	6
1.6.1 Registration templates	7
1.6.2 Normalization toolboxes:	8
1.6.2.1 SPM	8
1.6.2.2 DARTEL	8
1.6.2.3 ANTs	9
1.7 Spatial smoothing	9
1.8 Intersubject correlation toolbox	10
2 Method	12
2.1 Participants	12
2.2 Procedure	13
2.3 Relevant image acquisition	14
2.4 Preprocessing and Spatial Registration (Normalization)	14

2.4.1	SPM12	15
2.4.2	DARTEL	15
2.4.3	ANTs	16
2.5	Spatial smoothing	16
2.6	Inter-subject correlation analysis	17
2.7	Dice Similarity Coefficient	17
3	Results	19
3.1	Evaluating suprathreshold voxels	19
3.2	Evaluating high ISC values	21
3.3	Evaluating the pattern of intersubject correlation	24
3.4	Investigating the similarity in patterns of correlation across normalization meth-	
	ods	28
4	Discussion	30
4.1	Discussion and conclusion	30
4.2	Limitations	33
4.3	Future directions	34
	Bibliography	35
5	Appendix	41
	Appendix	41
	Curriculum Vitae	51

List of Figures

1.1	A) ISC in typical slices through the brain at each of the three cardinal orientations for the movie clip “Alfred Hitchcock presents: Bang you’re dead!”B) The extent of ISC evoked by four different films: Alfred Hitchcock presents: Bang you’re dead!”(green), Sergio Leone's The Good, the Bad and the Ugly (blue), Larry David's Curb Your Enthusiasm (red), and the unedited, one-shot segment-of-reality video filmed in Washington Square Park (orange). Modified from [1].	4
3.1	Proportion of voxels with ISC (r- value) ≥ 0.15 , for the “junior”group as a function of smoothing kernel width. There are no error bars, since there is a single observation for each of the 22 conditions. Label abbreviations: ISC- intersubject correlation; ANTs- Advanced Normalization Tools; SPM- Statistical Parametric Mapping; DARTEL- Diffeomorphic Anatomical Registration Through Exponentiated Lie Algebra.	21
3.2	Proportion of voxels with ISC (r- value) ≥ 0.15 , for the “community”group. There are no error bars, because there is a single observation for each of the 22 conditions. Label abbreviations: ISC-intersubject correlation; ANTs- Advanced Normalization Tools; SPM- Statistical Parametric Mapping; DARTEL- Diffeomorphic Anatomical Registration Through Exponentiated Lie Algebra.	22
3.3	Proportion of brain exhibiting ISC higher than the threshold in the “junior”group for the three different types of registration tools (SPM12, DARTEL and ANTs) when a)8mm FWHM, b)10mm FWHM, c)12mm FWHM, d)14mm FWHM, e)16mm FWHM and f)20 mm FWHM smoothing was applied. There are no error bars, because there is a single observation per data point. Label abbreviations: ISC-intersubject correlation; ANTs- Advanced Normalization Tools; SPM- Statistical Parametric Mapping; DARTEL- Diffeomorphic Anatomical Registration Through Exponentiated Lie Algebra.	23
3.4	Proportion of brain exhibiting ISC higher than the threshold in the “community”group for the three different types of registration tools (SPM12, DARTEL and ANTs) when a)8mm FWHM, b)10mm FWHM, c)12mm FWHM, d)14mm FWHM, e)16mm FWHM and f)20 mm FWHM smoothing was applied. ANTs yielded a higher proportion of voxels with correlation values over 0.15 at all smoothing levels. There are no error bars, because there is a single observation per data point. Label abbreviations: ISC-intersubject correlation; ANTs- Advanced Normalization Tools; SPM- Statistical Parametric Mapping; DARTEL- Diffeomorphic Anatomical Registration Through Exponentiated Lie Algebra.	24

3.5	Three cross-sections of the mean ISC values generated using three different registration techniques (ANTs, SPM12 and DARTEL) shown at x=60, y= -26, and z=4 in the MNI coordinate frame when 12mm kernel of smoothing was applied. Data are thresholded at a correlation value of r = 0.15. The left column corresponds to mean ISC values generated when data were normalized using DARTEL toolbox, the middle column demonstrates ANTs warped data and the right column demonstrates SPM12 warped data. As is shown, the region of highest correlation is around the superior temporal gyrus, bilaterally in all cross-sections. Label abbreviations: ANTs- Advanced Normalization Tools; SPM- Statistical Parametric Mapping; DARTEL- Diffeomorphic Anatomical Registration Through Exponentiated Lie Algebra	26
3.6	Three cross-sections of the mean ISC values generated using ANTs registration techniques shown at different MNI coordinate frames when 12mm kernel of smoothing was applied. Data are thresholded at a correlation value of r = 0.15.	27

List of Tables

2.1	Participants characteristics. Abbreviations: F = female; M = male; R = right; L = left.	13
3.1	Total number of brain voxels. Label abbreviations: ANTs- Advanced Normalization Tools; SPM- Statistical Parametric Mapping; DARTEL- Diffeomorphic Anatomical Registration Through Exponentiated Lie Algebra.	20
3.2	The Dice Similarity Coefficient for the binarized ISC maps, SPM12-ANTs, SPM12-DARTEL and ANTs-DARTEL at kernels of 8, 10, 12, 14, 16 and 20 mm FWHM of smoothing. The largest similarity index is between ANTs and DARTEL (higher than between ANTs and SPM12, and SPM12 and DARTEL) at 20 mm FWHM smoothing, for the “junior”group, and this pattern is evident in the “community”, suggesting that the results are reliable. Label abbreviations: ISC-intersubject correlation; ANTs- Advanced Normalization Tools; SPM- Statistical Parametric Mapping; DARTEL- Diffeomorphic Anatomical Registration Through Exponentiated Lie Algebra.	29

List of Appendices

Appendix A: Frequency of voxels exhibiting different ranges of ISC - whole data	42
Appendix B: Frequency of voxels exhibiting different ranges of ISC- junior group	43
Appendix C: Frequency of voxels exhibiting different ranges of ISC- community group .	44
Appendix D: Proportion of voxels exhibiting high correlation value for different levels of smoothing- whole data	45
Appendix E: Proportion of voxels exhibiting high correlation value for different levels of smoothing- junior group	46
Appendix F: Proportion of voxels exhibiting high correlation value for different levels of smoothing- community group	47
Appendix G: Research-ethics board approval	48
Appendix H: REB- Present investigation	49
Appendix I: Research ethics	50

Chapter 1

Introduction

Surgery is a promising treatment option for a significant number of patients with brain tumours or focal drug-resistant epilepsy [2]. Assessment of cortical function before surgery can aid in surgical planning in a number of ways - for example, by helping to localize dysfunctional cortex or to identify dysfunctional networks, and/or assess functional plasticity. Presurgical assessment of cortical functioning plays a critical role in minimizing postoperative morbidity and improving surgical outcomes for these patients [2]. MRI is commonly used to identify and localize any focal abnormality, which in about one-third of surgical candidates is subtle and not evident on clinical MRI [3]. More sensitive tools for identification of abnormality, potentially using functional criteria, are needed. In this thesis I focus on optimizing registration of data between an individual and a template. Optimizing the registration maximizes sensitivity of the movie-fMRI paradigm. So, this novel method of detailed functional mapping of the brain can be used for presurgical assessment in epilepsy. This study is the first study that uses a movie-fMRI paradigm to evaluate different registrations.

1.1 Presurgical assessment in Epilepsy

Epilepsy is a disorder characterized by at least one of the following conditions: “1) at least two unprovoked or reflex seizures more than 24 hours apart, 2) one unprovoked or reflex seizure and a probability (60%) of having another seizure similar to the general recurrence risk after two unprovoked seizures over the next 10 years, or 3) diagnosis of an epilepsy syndrome” [4]. Epilepsy is considered drug-resistant (DRE) when at least two categories of anti-epileptic medication are tried and tolerated on an appropriate schedule, but the patient still experiences seizures [5]. In DRE patients due to an abnormality in a discrete region (the epileptogenic focus), surgical removal of the focus can be an effective treatment [6] [7].

During a surgical resection for the treatment of epilepsy, surgeons try to remove as much diseased tissue as possible while preserving normal brain function. Careful localization of the

pathological tissue and comprehensive cognitive assessment are essential parts of the presurgical assessment. The former leads to a better medical prognosis (e.g., greater likelihood of seizure freedom in patients with refractory epilepsy), and the latter allows for better prognostication of likely cognitive deficits after surgery. The risk of an undesired effect must be weighed against the potential benefits of surgery, and the surgical team must predict the functional outcome based on the regions of the cortex to be resected.

The epileptogenic focus is localized by obtaining the neurological and general medical history, through electroencephalography (EEG) and through video EEG which reveals semiology at seizure onset, with potentially localizing significance. Brain imaging using magnetic resonance imaging (MRI) to detect structural abnormalities is also essential. Positron Emission Tomography (PET) and Single Photon Emission Computerized Tomography (SPECT) are also often used to visualize changes in cerebral metabolism [2]. In up to one-third of patients being considered for surgery, these investigations do not definitively locate the focus of abnormal activity. In this case, patients undergo invasive procedures like intracranial EEG (iEEG), which involves direct recording from the pial surface of the brain, to locate the focus of abnormal electrical activity. Monitoring brain activity through iEEG is not only invasive and needs hospital admission, but also expensive and carries risks [8].

In order to avoid undesirable cognitive changes postoperatively, and have a qualitative baseline measure of cognitive function, the language and memory functions are often characterised neuropsychologically, and sometimes evaluated using functional MRI and/or amytal hemispheric anesthesia (Wada test) during presurgical evaluation [9] [10]. Wada test is operationally defined by injection of sodium amytal into the internal carotid artery to induce hemianesthesia temporarily [11]. Due to the high possibility of some degree of brain reorganization of cognitive function in people with epilepsy, particularly those with seizures dating from birth or early life, individual functional mapping is desirable for many patients [12]. Wada and fMRI are typically used to characterize memory function, and to lateralize language. My project is focused on optimizing volume-based preprocessing of imaging data for a new method of presurgical functional assessment using neuroimaging.

1.2 Functional Magnetic Resonance Imaging

Functional MRI is a non-invasive neuroimaging method sensitive to brain activity, based on blood oxygen level-dependent (BOLD) signal changes. Magnetic susceptibility to alterations in the concentration of deoxyhemoglobin, blood flow, blood volume and the venous reservoir of the local brain tissue is the basis of BOLD-contrast imaging [13]. In fMRI experiments, different stimuli are used to elicit hemodynamic activity, which is then captured by the scanner as a proxy measure for neuronal activation. Any neuronal activity results in recruitment of oxygenated blood, which results in an increase in the concentration of local oxyhemoglobin rel-

ative to local deoxyhemoglobin. Since deoxyhemoglobin is strongly paramagnetic, and causes magnetic field distortions, the decreased proportion results in a more uniform magnetic field strength, and therefore increased signal on an image [13].

There are two general protocols for fMRI. In resting-state fMRI (rs-fMRI) brain dynamics are captured while subjects are at rest in the scanner. In task-based fMRI individuals are not simply resting, but are typically engaged in some kind of cognitive task. Verb generation and verbal fluency are the most common fMRI paradigms for presurgical mapping of language [9] [14]. However, these paradigms generally focus on single aspects of cognition, and do not reflect the richness of everyday language processing and cognition. As a result, they offer an incomplete view of cortical functioning. In addition, sometimes, the amount of movement in the scanner is too high to be corrected when preprocessing the data for analysis [14].

1.2.1 Movie-fMRI

To gain a more comprehensive view of cognitive function presurgically, and to reduce movement, we present engaging movies. The movie-fMRI paradigm resembles a natural viewing experience [1]. Because the task is simple and enjoyable, this paradigm can also be used effectively with children. Any silent movie or movie that contains audio can be selected based on the study's goal. For instance, if investigating the auditory cortex is desired the movie should contain audio and if the focus is explicitly investigating the visual cortex employment of a silent movie might be necessary. Previous studies have shown that participants move less in movie fMRI paradigms compared to resting-state paradigms [1].

1.3 Inter-subject correlation basics

When healthy individuals watch a naturalistic stimulus like a movie, extensive cortical areas (60 % of brain cortex) show robust hemodynamic activity that is time-locked to the content of the movie, and is synchronous across individuals [1]. Measuring this synchrony by means of fMRI, through the correlation of the BOLD signal time course in homologous voxels across viewers, is the basis of inter-subject correlation (ISC) analysis [15], which reveals that large regions of cortex exhibit high correlation in healthy individuals. ISC offers a way of quantifying the reliability of cortical activation across healthy individuals at the voxel level, with higher ISC values suggesting a more predictable time course of activation.

ISC analysis was initially proposed by Uri Hasson [15] for use with fMRI data from naturalistic stimulation paradigms such as movies. In ISC analysis, the time course of activation in each voxel of a given subject is correlated with the time course of activation of the correspond-

ing voxel in all other subjects, and then the correlation values are averaged. This is repeated for all subjects, and a grand average correlation is calculated [16].

1.4 “Bang You’re Dead!”

For this project, the naturalistic stimulus that we selected was an eight-minute long edited version of a black-and-white television episode, entitled “Alfred Hitchcock presents: Bang You’re Dead!”(1961). According to previous studies [1] [17] this movie is capable of robustly activating more than 60% of the brain cortex synchronously across individuals (resulting in high ISC values), including in areas of the brain that are not reliably activated by other movie stimuli (e.g., prefrontal cortex)(Figure 1.1) [1].

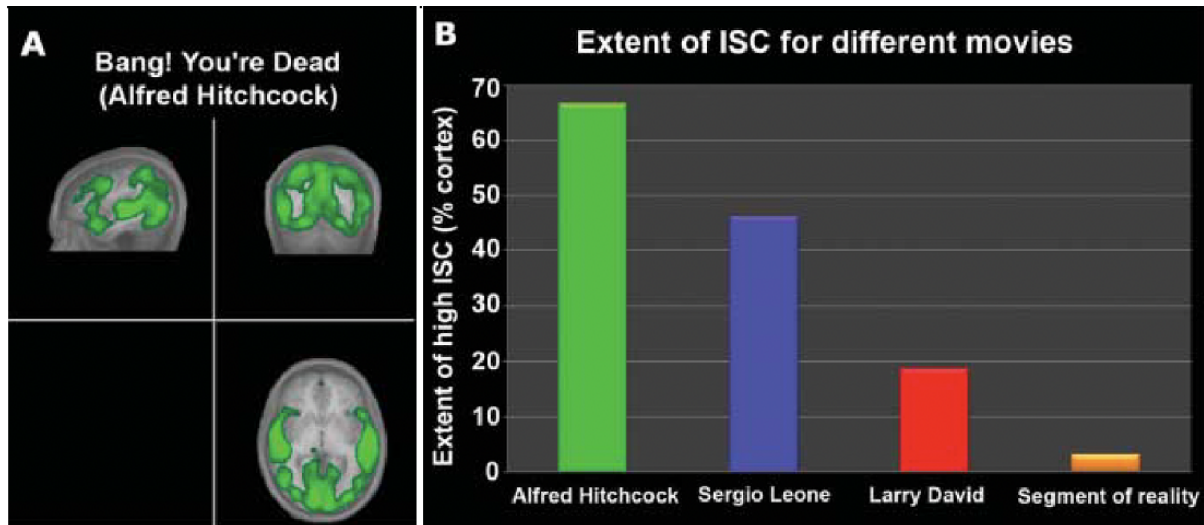


Figure 1.1: A) ISC in typical slices through the brain at each of the three cardinal orientations for the movie clip “Alfred Hitchcock presents: Bang you’re dead!” B) The extent of ISC evoked by four different films: Alfred Hitchcock presents: Bang you’re dead!”(green), Sergio Leone’s The Good, the Bad and the Ugly (blue), Larry David’s Curb Your Enthusiasm (red), and the unedited, one-shot segment-of-reality video filmed in Washington Square Park (orange). Modified from [1].

In this project, we used movie-driven fMRI to functionally map the cortex in healthy participants. This dataset can serve as a normative sample, against which to compare data from individual patients. Among individuals with neurological disorders, we can search for voxels that do not show the expected time course of activation, suggesting a focal functional or network abnormality. In individuals with neurologic disorders, identifying voxels or regions with a different signal pattern, as a result of focal functional impairments or functional reorganization, may help guide the health care team to the pathological areas. This technique may be

particularly valuable in cases of non-lesional epilepsy, in whom the structural neuroimaging is unremarkable [3] [18].

1.5 Anatomical variability and processing of the fMRI data

There are normal variations in human brains in the size and shape and in the minute detail of sulci and gyri arrangement [19]. For example, the primary auditory cortical receiving area (from thalamus) is always found on Heschl's gyrus on the superior temporal plane. In some people there is only one Heschl's gyrus in each hemispheres. Other individuals may have up to three separate Heschl's gyri, in either or both hemispheres [20]. These variations complicate the voxel-wise correlation across individuals and can significantly reduce correlation values [21] [22]. These challenges can be mitigated by normalization and spatial smoothing. Normalization algorithms that can accommodate the detailed anatomical morphology of individual brains have been shown to reduce variability, and as a result improved the anatomical alignment across groups [22] [23]. Enhancement in structural overlap may increase functional overlap: it improves overlap in resting state networks across individuals [23], and in activation clusters in primary sensory areas [24]. This overlap may also enhance intersubject correlation (as we examine here) .

In the preprocessing of fMRI (1) brains are registered to standard space (spatial normalization) to reduce the variability across people [25], and (2) data are spatially filtered (smoothed) to maintain a balance between data resolution and signal sensitivity and anatomical correspondence across individuals [26] [21]. These preprocessing steps should improve reliability across subjects and statistical power, so that, when used as a norm against which to compare patients (assuming grossly normal brain morphology), we will be more sensitive to abnormality.

Normalization and smoothing render anatomically different brains more comparable. Normalization registers brains together in a standard space, so that an individual patient brain corresponds to that of a normative template.

Spatial smoothing works to diminish residual anatomical variability after normalization, at the cost of degrading spatial resolution. According to theory of matched filters, the optimal amount of spatial smoothing that maximizes the signal to noise is that which matches the size of the activated region [27].

I aim to enhance the strength of fMRI-derived ISC to improve the sensitivity of noninvasive presurgical evaluation procedures to detect focal functional abnormalities, with the ultimate goal of reducing the need for invasive procedures.

ISC values are influenced by multiple factors including sample size [28], level of spatial smoothing [21], and variations in brain morphology [29]. Optimizing any of these factors would probably enhance the strength of the ISC values and the consequent sensitivity of this method to brain functional abnormality. In this study, I use movie-driven fMRI to evaluate the registration algorithms and smoothing level that yields greatest overlap in individuals, indexed as ISC values. The three different normalization toolboxes are open-source and include the regular normalization algorithm of the commonly used image processing toolbox, SPM [30] version 12, developed in the Wellcome Trust Centre for Neuroimaging, University College London, UK; the DARTEL [31] toolbox; and the ANTs toolbox, developed by members of PENN image Computing and Science Lab (PICSL) and other institutions led by Brian Avants at University of Pennsylvania, Philadelphia, PA, US [32]. I use volumetric normalization here and did not attempt surface based registration, for reasons that I explain in the Discussion. In the following sections, spatial normalization and spatial smoothing will be discussed in detail.

1.6 Normalization

In order to compare the ISC of different brains of different sizes and morphology, they should be brought into a standard space [33]. The spatial transformation of data images into a standardized template is called “individual registration” [33] or spatial normalization. During normalization, the high-resolution anatomical image is registered to the template of choice. Transformation parameters derived from this registration, which are discussed later in this section in more detail, are then applied to each functional image volume. Several normalization procedures are available.

Different normalization methods are categorized based on whether they are volume-based or surface-based normalization. The volume-based normalization involves registration of a three-dimensional volume of the whole brain into a standard template [34], based on the differences in the intensity of data [35]. Surface-based normalization involves segmenting brain images and virtually flattening cortex, then registering cortical maps onto a set of two dimensional standard templates. Because surface-based normalization is not used in this thesis, it will not be discussed in detail. In this work, we compare three volumetric template-based normalization methods.

The registration algorithms differ based on whether the registration requires a standard reference template (such as the MNI-ICBM 152 template [36]) or involve registering all images together in a single procedure (groupwise registration).

Normalization methods are categorized into affine transformations and non-affine non-linear transformations. Affine transformations applied to the whole brain volume (either with a reference template or among a group of volumes) consist of rigid-body transformations, in-

cluding rotations (yaw, pitch, and roll) and translations in three main axes (x, y and z) for each. Affine non-rigid-body transformations include scaling and shearing (skewing): these are typically also applied to data on top of the rigid body transformation parameters .

Non-affine non-linear transformations, if performed, generally follow linear and nonlinear affine transformations. In contrast to the affine transformations, the non-affine nonlinear transformations differ in different regions of the brain. These can be either smoothly nonlinear, with a low number of degrees of freedom: in such cases, nonlinear warpings are applied on relatively large regions of tissue. Alternatively, these may be highly nonlinear, with a large number of degrees of freedom, enabling one brain to be warped to be almost identical to another at a relatively fine anatomical scale. High-dimensional nonlinear transformations are useful for minimizing individual anatomical variability among brains. It is unclear to what extent such transformations maximize functional overlap among individuals, however, since function does not necessarily follow form, particularly in frontal and parietal regions [29] [37]. I will utilize both low-dimensional and high-dimensional nonlinear normalization methods, and assess whether a measure of functional alignment, ISC, is more widespread after the latter than the former.

All three volume-based normalization toolboxes apply the non-linear approach in the registration of image data, but they vary in the degree of transformation that they implement. The SPM toolbox implements a smoothly non-linear algorithm with low degrees of freedom (around 1K). DARTEL uses larger deformations (more degrees of freedom (6.4 M)) than the conventional SPM normalization [37] [38]. ANTs is a robust nonlinear registration toolbox that applies nonlinear transformation parameters (stretching and squeezing) at an even finer spatial scale (28 million degrees of freedom), so that the transformed image is more similar to the template [37].

1.6.1 Registration templates

Different versions of the MNI-ICBM template generated by researchers at the Montreal Neurological Institute (MNI) under the aegis of the International Consortium for Brain Mapping (ICBM) [36] are the standard templates of choice for most of the normalization toolboxes [39] including Statistical Parametric Mapping (SPM) and Advanced Normalization Tools (ANTs) [32]. The MNI-ICBM template was first created in 1992 out of an average of T1 weighted data images of 305 normal brains [40]. Currently, more updated versions of this template are available with different voxel size resolutions. The MNI-ICBM-152 is the one implemented in SPM 12 and in the ANTs pipelines. These templates are generated from a population of healthy young individuals; thus, they might not represent changes in brain morphology for individuals of different ages or from various ethnicity groups. In contrast, groupwise normalization optimizes the match among all the brain volumes in a given sample, and thus is more

robust to alterations. The DARTEL toolbox uses a groupwise template created by simultaneously registering all the constituent images together. This theoretically eliminates bias caused when samples used to create a standard reference template are different (e.g., younger) than those in the experimental sample.

1.6.2 Normalization toolboxes:

1.6.2.1 SPM

SPM has been designed for the investigation of multiple modalities of brain imaging data [30]. The latest version (12th) of the software was released in 2014. SPM is designed for the analysis of fMRI, EEG, PET, SPECT, and MEG. SPM incorporates many routines for the processing of brain imaging data. Here, we concern ourselves with the normalization algorithm, which is a voxel-based, low dimensional (1K degrees of freedom) [37], volume-based registration [37]. The SPM algorithm minimizes the voxel-wise squared difference between the volume images and a template volume, which is MNI-152 standard template [37]. The standard SPM non-linear normalization involves application of two main steps: 12- parameter affine registration (translations, scaling and shears in x y and z, and pitch, roll, and yaw) followed by the application of a weighted sum of cosine basis functions [41] [42].

By performing “unified segmentation” [43], according to a tissue probability map, the image data [43] are segmented into the six different tissues of white matter (WM), gray matter (GM), cerebrospinal fluid (CSF), bone, soft tissue, and background. The segmented tissues are then used to determine the deformation parameters by warping the template data to match an individual’s data. Finally, each subject’s images are spatially warped, using the inverse of previously defined deformation parameters [43] [37] [38].

1.6.2.2 DARTEL

The Diffeomorphic Anatomical Registration Through Exponentiated Lie Algebra (DARTEL) toolbox is a volume-based normalization choice in SPM packages. This was proposed by Ashburner in 2007 and is a diffeomorphic image registration method. The diffeomorphic transformations, are defined as “topology preservation”, which is crucial when mapping cognitive function to cortex [44]. DARTEL is a high dimensional(6.4 million degrees of freedom) [37], non-linear spatial registration toolbox, which exploits groupwise registration.

Similar to the SPM registration algorithm, DARTEL applies tissue segmentation. The average intensity of the WM and GM comprises the initial template in DARTEL. The initial

template is updated repeatedly until a sharp, spatially precise template is built for the subject group. The final average template is used for registration of each subject's dataset.

1.6.2.3 ANTs

The registration algorithm in the ANTs software package is a high dimensional (28 million degrees of freedom) [37], non-linear, diffeomorphic, volume-based normalization that registers image data to the standard MNI-152 template [32]. The ANTs algorithm has been compared to other normalization methods in previous work, and has performed the best among 14 registration algorithms based on different measures, including “volume and surface overlap, volume similarity, and distance measures” [37].

We used version 2.2.0 of this software package for spatial normalization of the data [32]. The most common non-linear registration algorithm in ANTs software package is normalization” (SyN) [37]. Like other normalization toolboxes, segmentation is a necessary step before normalization, and this is accomplished via FSL [45]. Then for each individual, spatial normalization to the MNI-ICBM 152 template was performed using ANTs' antsRegistration in a multiscale, mutual-information based, nonlinear registration scheme [32]. The deformation parameters derived for the structural were then applied to coregistered functional data [32].

1.7 Spatial smoothing

Spatial smoothing involves blurring signal across adjacent voxels. Spatial smoothing is commonly performed using a three-dimensional Gaussian filter. The degree of smoothing is proportional to the full width at half maximum (FWHM) of the Gaussian distribution, and this, together with the voxel resolution, determines the spread of the signal over voxels. Smoothing is performed for three main reasons. It decreases the effect of anatomical variability across subjects, and therefore increases overlap in functional activation across participants, it increases signal to noise ratio, and it is essential in some types of statistical analysis when the assumptions of random field theory (RFT) need to be met to correct for multiple comparisons [19]. When RFT is required, the appropriate level of smoothing is two or three times the voxel size [21]. As mentioned earlier, in theory, the optimal amount of spatial smoothing is that which matches the size of the activated region [27], but since this is rarely known in advance, smoothing between 6 and 12 mm is typical, depending on the goal of the study [46][19].

In movie-fMRI, ISC analysis instead of conventional general linear model (GLM), is the analysis method of choice, and RFT is not required. Pajula and his colleagues showed that when conducting an ISC based analysis on fMRI data, applying a kernel filter with the size of 8 to 12 mm FWHM, produced the highest number of voxels exhibiting a significant cor-

relation value, and generally higher correlation values [19][21]. However, spatial smoothing degrades functional resolution, and the function relating improvement in correlation values to smoothing kernel size is typically compressive, yielding progressively smaller improvements. In this work, we will attempt to find the optimal smoothing level. We expect to find that high smoothing levels will lead to stronger, more reliable correlations, but will attempt to identify the smoothing level at which improvements in correlation diminish for increasing filter widths, so as not to compromise spatial resolution unduly.

The application of spatial smoothing will affect both the apparent spread of synchronization of the brain signal activity and the magnitude of (peak) synchronization. In fact, smoothing will confound magnitude with extent. With smoothing, an intense but focal peak will become smeared, and indistinguishable from a less focal peak of lower magnitude. Thus, one must be cautious when interpreting proportions of voxels exhibiting correlation above a particular threshold, across different levels of smoothing. This proportional value will increase with increased smoothing. For this reason, the extent of correlation clusters is not a sufficient measure – the peak correlation value must also be considered, and the proportion of voxels exhibiting relatively high correlation. In our study, six different levels of spatial smoothing (8mm,10mm, 12mm, 14mm,16mm and 20mm FWHM) were applied to the data, after normalization.

1.8 Intersubject correlation toolbox

In this project, a commonly used open-source MATLAB-based ISC toolbox designed by the Department of Computer Science and Helsinki Institute of Information and Technology (HIIT) University of Helsinki, Helsinki, Finland is employed. For each subject, the ISC toolbox calculates the Pearson correlation coefficient – ISC - of the fMRI time courses, in corresponding regions (voxels). ISC values were determined separately based on the data output from each of the different normalization toolboxes per level of smoothing. Then the ISCs were evaluated based on the proportion of voxels with ISC values exceeding the defined threshold of 0.15 (or the average of ISC values across voxels for each individual) [47]. By identifying the normalization method and the level of smoothing that reliably yields the strongest ISC, with a robust spread, I will identify the optimized combination for the most sensitive ISC.

The current study used a movie-fMRI paradigm and applied an ISC based analysis to identify the combination of spatial registration and spatial smoothing (using three different volumetric normalization algorithms and six different levels of spatial smoothing) that maximizes the magnitude and extent of ISC in the brain. The analysis is conducted on two independent samples – one of university students, and one of community-dwelling adults matched in age to a clinical population – to examine the reliability and generalizability of the results. The pattern of ISC resulting from the combination of choice for the preprocessing of movie-driven fMRI data, particularly in the community sample, can serve as a normative pattern of activity, and the normalization/smoothing combination identified here will be used in the presurgical as-

assessment of patients with neurological disorders, to ensure that sensitivity is as high as possible.

Chapter 2

Method

In this section, I first describe participants, the study procedure, and then the image acquisition settings. The preprocessing and registration steps are explained separately for each toolbox SPM, DARTEL, and ANTs. Finally, the intersubject correlation analysis (ISC) and other statistical analyses are discussed.

2.1 Participants

Forty-four neurologically healthy individuals (age range = 17 - 61 years old; mean = 29.4 years; 28 females; 4 left-handed), participated in the study. General inclusion and exclusion criteria were assessed at a pre-screen phone interview.

Participants were recruited as two subgroups (n=22) of the “community” group (age range = 17 - 61 years old; mean = 35.7 years; 14 females; 4 left-handed) and the “junior” group (age range = 18 - 30 years old; mean = 23.2 years; 14 females; all right handed). The “community” group were recruited from the University of Western Ontario (UWO) and greater London community through flyers and advertisement in clinics, the “junior” group were recruited from among the undergraduate population at University of Western Ontario. The two groups of participants were analyzed separately so that I could assess the reliability and generalizability of the results.

All subjects were fluent in English and able to understand and follow a narrative audiovisual movie clip. They were comfortable lying in the scanner for approximately half an hour. None reported claustrophobia or any other contraindication to being exposed to a strong magnetic field, based on the MR safety screening form, and no participant regularly used medication that alters one's mental status or level of consciousness such as benzodiazepines or opioids.

	Whole data	Community data	Junior data
N	44	22	22
Sex (F:M)	28:16	14:8	14:8
Age (M \pm SD)	29.4 \pm 12.4	35.7 \pm 14.9	23.2 \pm 3.2
Handedness (R:L)	40:4	18:4	22:0

Table 2.1: Participants characteristics. Abbreviations: F = female; M = male; R = right; L = left.

Details of the procedure were explained to participants. Informed consent was obtained prior to the study. Ethical approval was obtained from the Health Sciences Research Ethics Board of the University of Western Ontario (Appendix G). These data were part of a larger neuropsychological study, which also involved taking a general medical and medication history, and collecting psychological measures including Beck's depression inventory, measures of anxiety, depression, sleep quality, quality of life and measures of verbal and nonverbal memory (WMS-III) [48]. These measures will not be discussed in the current work.

2.2 Procedure

After 30 minutes of pretesting in which the psychological measures mentioned above were administered, individuals who needed correction for visual acuity were provided with corrective lenses mounted on an MRI compatible frame according to their prescription values and comfort level and made comfortable in the 3 Tesla Siemens Prisma MR imaging scanner system.

Participants were asked to simply relax in a supine position, and stay still, while they were scanned. Two different MRI protocol sequences were followed: a) the “community” group protocol : T1-weighted structural MRI, fluid attenuation inversion recovery (FLAIR), diffusion tensor images (DTI) and fMRI. Functional MRI included a 6 minute, 33-second resting-state scan (with eyes closed) that was acquired before the movie acquisition for further possible analysis, b) the “junior” group protocol: T1-weighted structural MRI and fMRI. Functional MRI included two sets of two different audiovisual movie clips, 8 minutes long each, and 12 minutes of resting-state scan (with eyes closed) that was acquired in between the two movie acquisitions for further possible analyses.

The final audio-visual movie clip in both protocols was an eight-minute edited version of the 1961 TV episode “Bang You’re Dead!” from the TV series “Alfred Hitchcock Presents!”, which was originally 22 minutes long [17] [49]. I analyzed data from the “Bang you’re dead!” clip, using the acquired T1-weighted structural MRI for image registration and localization.

Stimulus presentation was controlled by a custom MATLAB version 2015b script, (<http://mathworks.com>), and the movies were back-projected onto a screen behind participants' heads and reflected off mirrors into the participants' eyes. Noise cancelling, MR-compatible headphones (Sensimetrics, S14; www.sens.com) were used for sound delivery. Hearing comfort level was tested before starting the experiment and sound was presented at that comfortable level. Following the scan, volunteers were asked to recall the movie narrative, and then respond to some questions about the details of the movie [50]. Overall, the MR scan and memory tests took about one hour and 20 minutes of participants' time. The memory data are not analyzed here.

2.3 Relevant image acquisition

Only the data acquisition parameters relevant to this project are provided. The anatomical data were captured using a T1-weighted 3D rapid acquisition gradient echo (MPRAGE) sequence (32 channel coil, 1 x 1 x 1 mm voxel size, matrix size 240 x 256 x 192, 2300.0 ms repetition time (TR), 2.98 ms echo time (TE) and 9 degrees flip angle (FA)). Functional data were obtained using gradient echo (GRE) echo-planar imaging (EPI) (33 slices, voxel size 3 x 3 x 3mm, matrix size 192 x 192 x 123, interslice gap of 25%, 2000 ms repetition time (TR), 30 ms echo time (TE), and 75 degrees flip angle (FA), multi-band accelerator factor 2, Generalized Autocalibrating Partial Parallel (GRAPPA) for Parallel Acquisition Techniques (PAT) mode). Movie scans consisted of 246 volumes.

2.4 Preprocessing and Spatial Registration (Normalization)

In the following sections, I will first describe the initial preprocessing then I will detail how three different normalization methods were applied to the data. Lastly, I will describe the different levels of spatial smoothing and the intersubject correlation (ISC) analysis that I conducted.

All analysis steps were performed on a Linux operating system Ubuntu 16.04, LTS, Intel® Core i7-6700 CPU @ 3.40GHz 8, with 62.8 GiB memory and 8.8 TB disk capacity unless stated otherwise. A custom MATLAB 2017b (<http://mathworks.com>) software program was used for calling modules and performing the analysis.

The following preprocessing steps were applied on data for SPM12 and DARTEL toolboxes: Both the anatomical T1-weighted (T1w) images and functional BOLD images within the input data set of each subject were visually inspected for quality and the position of the

image origin. They were reoriented manually where necessary. If the origin of the data was 3-5 mm away from the anterior commissure of the brain (coordinates 0,0,0), the image volume was reoriented using the SPM toolbox. All images were then corrected for motion, realigned and resliced to correct the slice timing difference using the 'Realign: Estimate and Reslice' function of SPM12 [43]. The T1w images were coregistered to the corresponding functional data using 'coregister estimate and reslice' [43].

For the ANTs toolbox, all the preprocessing of the data and spatial registration were performed using fMRIPrep 1.1.8 [45], a robust, automated preprocessing workflow, designed by the Department of Psychology at Stanford University, California, USA, which is based on Nipype 1.1.3 [51] [52].

2.4.1 SPM12

Spatial registration of both T1w and BOLD data to the MNI-152 was performed using the 'normalization batch: estimate and write' module [43], as discussed in the introduction chapter. Using the 'check reg' utility of SPM12, and comparing multiple corresponding points such as ventricle borders or anterior and posterior borders of the corpus collosum, the quality of the spatial normalization was assessed against the MNI-152 template for quality control of the normalization step.

2.4.2 DARTEL

Normalization in DARTEL [31] comprised three separate steps: a) tissue segmentation for DARTEL import, b) template creation, and c) data registration [43].

The coregistered T1w images were segmented into different tissue classes within the following order: grey matter (GM), white matter (WM), cerebrospinal fluid (CSF), bone, soft tissue and air/background, according to a standard tissue probability map (tpm/TPM.nii) [43].

A set of template files were generated out of the segmented grey matter and white matter data of all subjects. As the registration progressed, the newly built templates became progressively sharper [43]. Finally, all the functional data were registered to the final custom template.

2.4.3 ANTs

For anatomical data the following preprocessing was applied. The T1-weighted (T1w) image was corrected for intensity non-uniformity [32], and used as T1w-reference throughout the workflow. The T1w-reference was then skull-stripped.

Spatial normalization to the MNI- ICBM 152 Nonlinear Asymmetrical template version 2009c [53] was performed through nonlinear registration (ANTs 2.2.0) [32]. Brain tissue segmentation of cerebrospinal fluid (CSF), white-matter (WM) and gray-matter (GM) was performed on the brain-extracted T1-weighted volume (FSL 5.0.9) [39].

For each of the BOLD runs per subject, the following preprocessing was performed. First, a reference volume and its skull-stripped version were generated (FMRIPrep) [45]. The BOLD reference was then co-registered to the T1w reference (FreeSurfer) [54]. Co-registration was configured with nine degrees of freedom to account for distortions remaining in the BOLD reference. BOLD runs were slice-time corrected [55]. The BOLD time-series were resampled onto their original, native space correcting for head-motion and susceptibility distortions, and resampled to the MNI152 standard space. Confounds in the time-series were calculated based on the preprocessed BOLD, and removed [56] [57]. The BOLD time-series were resampled to volumes using 'antsApplyTransforms' (ANTs) [32].

2.5 Spatial smoothing

The 'Smooth' module of the SPM12 was used to implement spatial smoothing at six different levels for SPM12 and ANTs warped image data: Gaussian kernels of 8mm, 10mm, 12mm (four times our voxel size), 14mm, 16mm, and 20mm full width at half-maximum (FWHM). The smoothing kernels of 8 through 12mm FWHM were chosen in agreement with [21]. The 14, 16 and 20mm FWHM filters were applied to investigate the effect of smoothing kernels beyond the previously investigated filtering levels. By including smoothing levels higher than optimal (and larger than the veridical size of underlying functional areas), it should be easier to identify the smoothing level that yields maximal ISC, assuming that matched filter theory applies to our data.

In the DARTEL algorithm, because a Gaussian kernel of 8mm FWHM of spatial smoothing was applied on data as part of the default setting parameter in the registration step [43], the FWHM of smoothing kernels were calculated accordingly. The final filter level (S) is the square root of the sum of the square of the two filter kernels (s1 and s2) :

$$S = \sqrt{(s1)^2 + (s2)^2}$$

To achieve 10mm FWHM, a kernel of 6mm FWHM was applied on data; applying 8.94 mm FWHM resulted in 12mm FWHM; applying 11.49 mm FWHM resulted in 14mm FWHM; performing 13.85 mm FWHM and 18.33 mm FWHM gave us 16 and 20mm FWHM of smoothing respectively.

2.6 Inter-subject correlation analysis

In order to find the areas with the highest degrees of shared hemodynamic activity, ISC analysis was performed using a MATLAB-based ISC toolbox developed by the Department of Computer Science and HIIT, University of Helsinki, Helsinki, Finland [16]. This ISC toolbox is designed to analyze fMRI data captured under naturalistic complex stimuli such as the movie we use here. Basic ISC analysis was performed on nifti output on each pair of participants, within each normalization method and each level of smoothing.

This involves calculating Pearson's correlation coefficients voxelwise between hemodynamic time series between pairs of participants [16]. Then, correlations across all pairs were averaged together voxelwise. This generated an average correlation map (nifti image) for each normalization method and each level of smoothing, creating 18 maps in total.

2.7 Dice Similarity Coefficient

I measured the spatial similarity of ISC patterns across normalization methods and smoothing levels, separately for the two subsamples of data (n= 22 subjects each) using dice similarity coefficient (DSC). The DSC index is a measure of spatial similarity of two binarized and thresholded maps. This will reveal whether different normalizations (and or different levels of smoothing) result in different ISC in different brain regions.

Using the 'ImCalc' module of the SPM12 toolbox, the ISC maps were binarized. A voxel's value was ascribed as one if the correlation value passed the threshold and otherwise as zero. The DSC was calculated using MATLAB 2017b ([http:// mathworks.com](http://mathworks.com)).

The DSC is defined as:

$$(2 * A \cap B) / (A + B)$$

Where A represents the binarized and thresholded first image (ISC map) and B represents

the binarized and thresholded second image (ISC map). The DSC index varies between 0, indicating no anatomical overlap between the two binarized images, and 1, demonstrating complete overlap (highest level of similarity) [58], or “Almost Perfect” agreement based on the Landis and Koch measure of agreement for categorical data [59].

Chapter 3

Results

The fMRI image data for all 44 subjects were included in the analysis. For each subject, the movie-driven functional data consisted of 241 volumes, after discarding the first five dummy files. In what follows, to ensure that my results are consistent, I first analyse the data from the 22-person “junior” group, and then examine whether the results replicate in the independent, 22-person “community” group. If they do, I conclude that the results are robust and at least somewhat generalizable.

In our study, the ISC was calculated by “computing the voxelwise correlation between each possible subject pair in the group of subjects ” [28], the method that is implemented in the ISC toolbox [16]. For each voxel, the individual's Pearson's correlation coefficient of the fMRI time series was calculated pairwise, and then these were averaged, similar to the method used by Pajula and his colleagues [28].

We first calculated the total number of voxels in ISC maps across the brain for every processing condition (Appendix A-C), so that we could then express the voxels exhibiting elevated correlation as a proportion of this value. In ISC map images, all voxels with absolute Pearson's correlation value larger than zero were counted across the brain mask. In all processing conditions, the ANTs toolbox yielded the largest number of brain voxels compared to the other two toolboxes (DARTEL and SPM12), across all smoothing conditions (see Table 3.1).

3.1 Evaluating suprathreshold voxels

We took the rather arbitrary value of 0.15 to serve as our threshold for meaningful correlation. Evaluating maps for statistically significant correlation would require a separate set of analyses involving correction for non-independence [60]. Since the goal here was simply to identify the

Normalization	Whole data	Community group	Junior group
DARTEL	220118	220118	227441
ANTs	219093	198971	220600
SPM12	196765	221062	211800

Table 3.1: Total number of brain voxels. Label abbreviations: ANTs- Advanced Normalization Tools; SPM- Statistical Parametric Mapping; DARTEL- Diffeomorphic Anatomical Registration Through Exponentiated Lie Algebra.

combination of normalization and smoothing that yields highest correlation values (regardless of actual significance; which depends on sample size and a host of other factors), we worked with this arbitrary value.

To evaluate the effect of different kernels of smoothing on ISC analyses, the proportion of voxels (relative to the total number of voxels in the brain) exhibiting correlation values larger than the threshold ($r=0.15$) in four different ranges of correlation (r -value) (between 0.15 and 0.20; between 0.20 and 0.25; between 0.25 and 0.30; and higher than 0.30) were compared at different levels of smoothing.

In the “junior” group, the relative proportion of voxels demonstrating suprathreshold correlation increased as smoothing increased across all normalization packages (Figure 3.1). The pattern of increase in voxel count was in accordance with other studies [21], in which an increase in smoothing expanded the activation sites and strengthened the synchronization level; as a result, the correlation values (r) rose [21] (Appendix D, E, and F; Figure 3.1). The slope of the increase was compressive, with the asymptote at approximately 12-14mm. ANTs and DARTEL seemed to yield somewhat higher proportions of voxels than SPM12 at the lower levels of smoothing (8-14 mm). No statistical analysis is possible here since there is only a single observation of proportion in each cell, but the difference between the proportions yielded by ANTs and DARTEL on the one hand, and SPM on the other, is approximately 20% at 8 and 10 mm of smoothing.

In the “community” group, similar to the “junior” group, the proportion of voxels increased steadily as smoothing kernel increased (see Figure 3.2). Again, the asymptote occurred at approximately 12-14 mm of smoothing. The overall proportions in this group were lower: at most 75% those of the “junior” group. Furthermore, in this group, a much more marked difference among normalization methods was observed, with ANTs yielding values almost 200% higher than SPM12 and DARTEL.

We next examined how the distribution of correlations differed as a function of smoothing and normalization method. In the “junior” group, the highest proportion of voxels was observed at the lowest ISC value category ($0.15 < r < 0.2$) (Figure 3.3), not surprisingly. The proportion of brain voxels generally dropped as the correlation values increased across all nor-

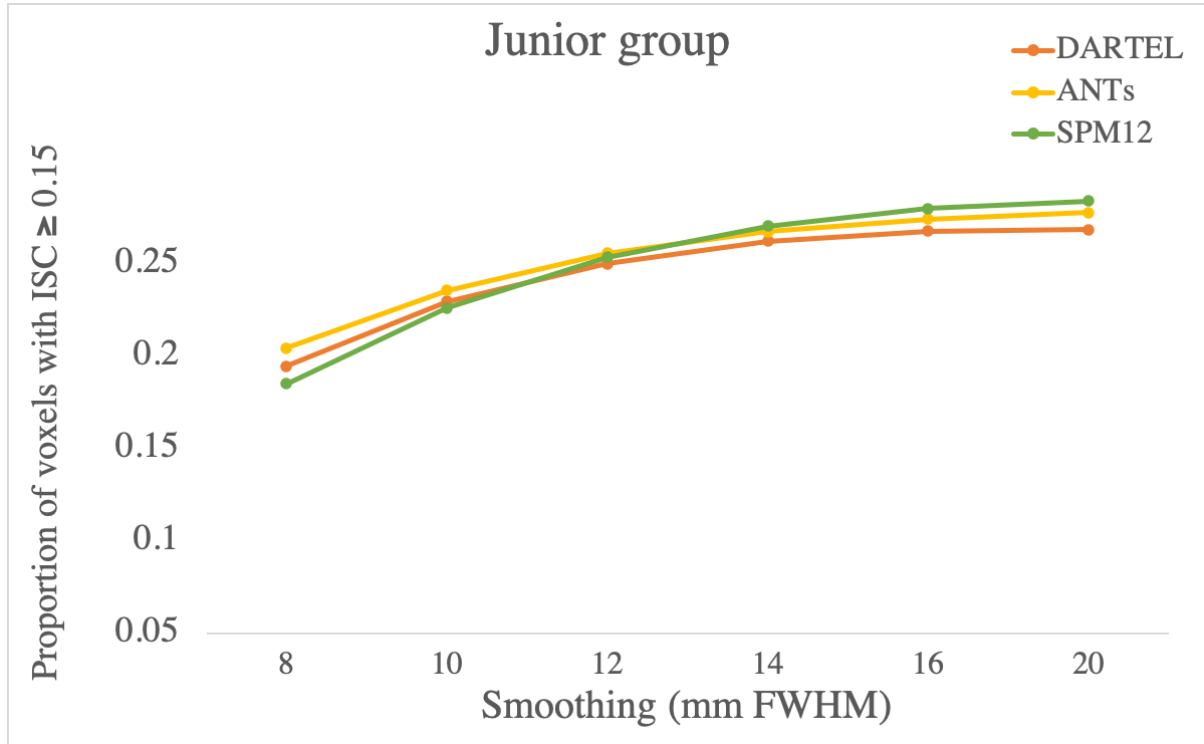


Figure 3.1: Proportion of voxels with ISC (r -value) ≥ 0.15 , for the “junior” group as a function of smoothing kernel width. There are no error bars, since there is a single observation for each of the 22 conditions. Label abbreviations: ISC-intersubject correlation; ANTs- Advanced Normalization Tools; SPM- Statistical Parametric Mapping; DARTEL- Diffeomorphic Anatomical Registration Through Exponentiated Lie Algebra.

malization toolboxes and smoothing kernels (Figure 3.3). There was a consistent tendency for SPM12 to yield a lower proportion of high correlation (>0.3) values compared to the other two normalization types.

The community group showed a broadly similar pattern to the junior group, with the proportion of brain voxels dropping as correlation values increased (see Figure 3.4). This group, however, appeared to differ from the junior group in how normalization affected the distribution of correlations over bins: ANTs yielded a higher proportion of voxels with correlation values over 0.15 at all smoothing levels in the “community” sample.

3.2 Evaluating high ISC values

Reviewing the proportion of brain voxels with ISC values (r) larger than 0.3, it was obvious that across all kernels of the smoothing, in both the “junior” group and the “community” group, the ANTs toolbox almost always outperformed DARTEL and SPM12 toolbox in that it reliably

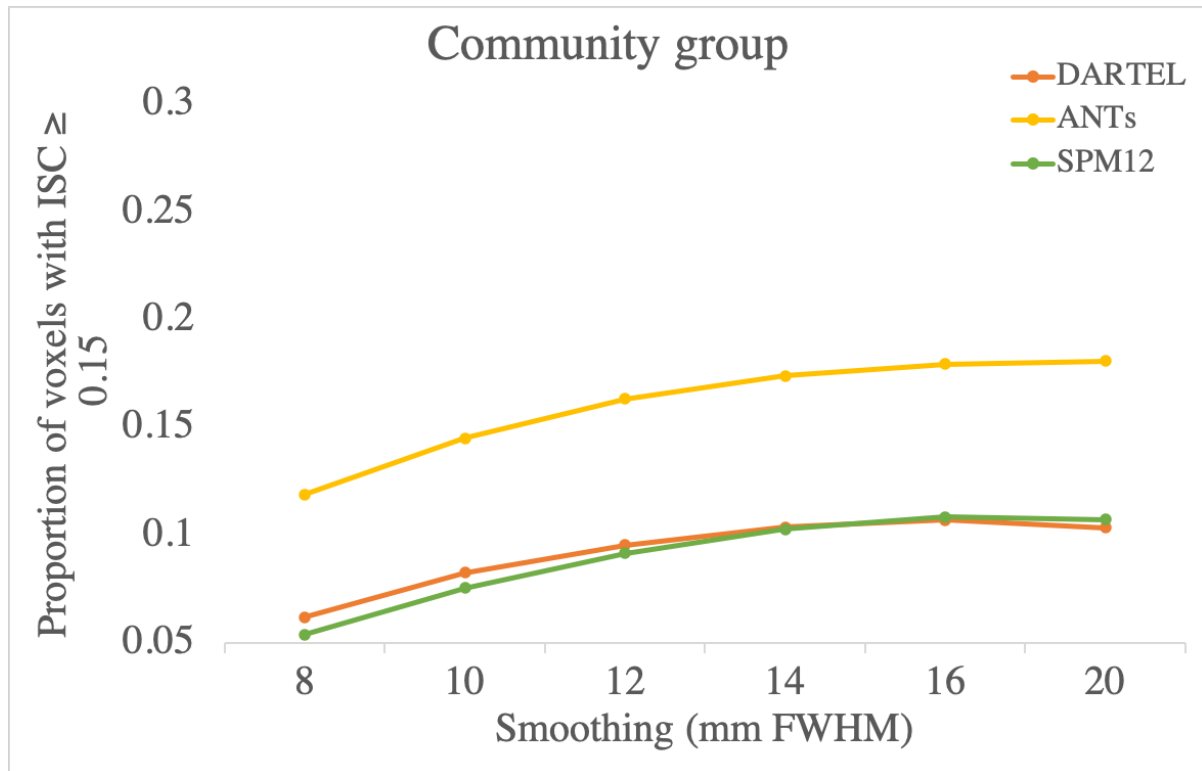


Figure 3.2: Proportion of voxels with ISC (r -value) ≥ 0.15 , for the “community” group. There are no error bars, because there is a single observation for each of the 22 conditions. Label abbreviations: ISC-intersubject correlation; ANTs- Advanced Normalization Tools; SPM-Statistical Parametric Mapping; DARTEL- Diffeomorphic Anatomical Registration Through Exponentiated Lie Algebra.

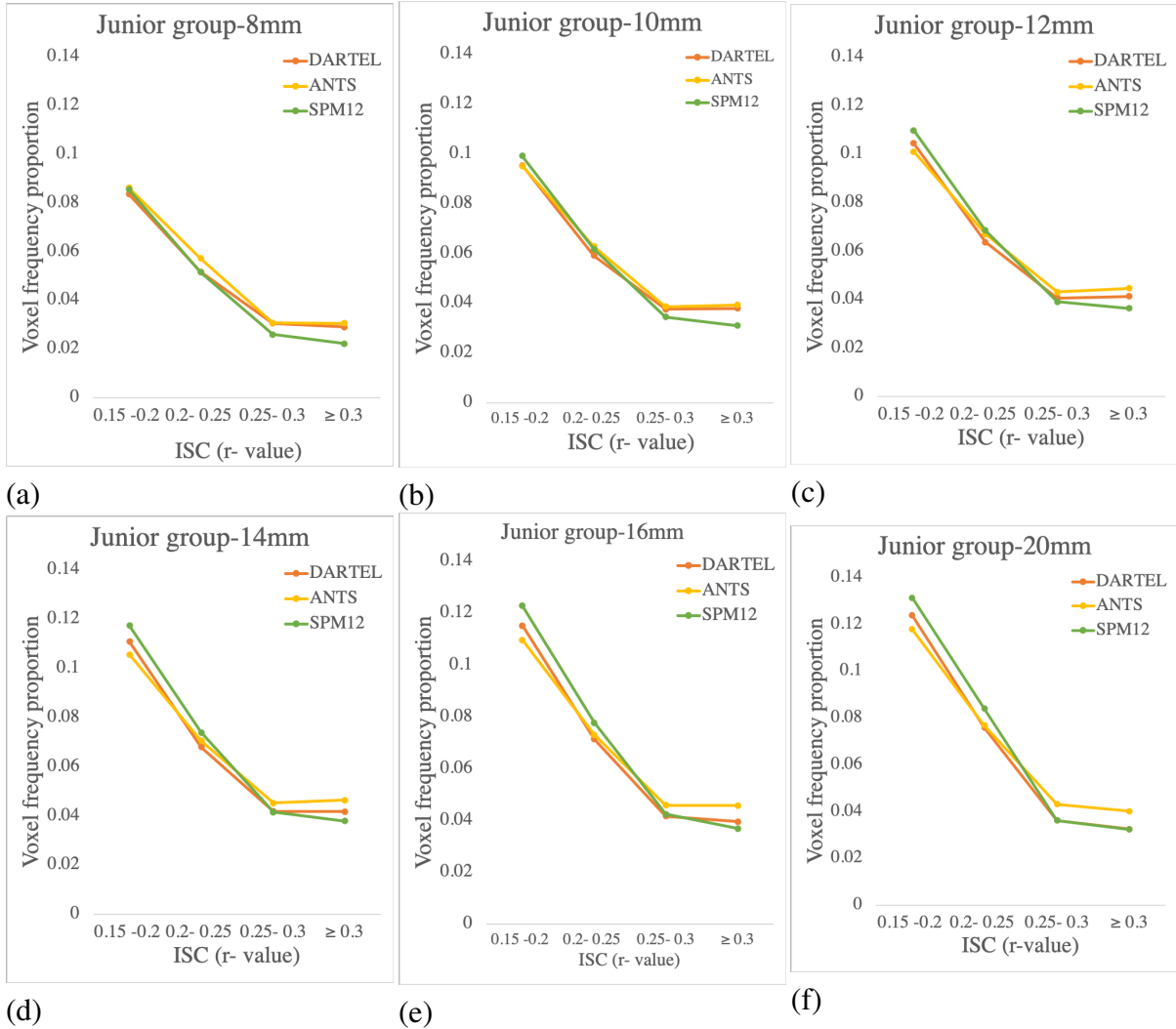


Figure 3.3: Proportion of brain exhibiting ISC higher than the threshold in the “junior ” group for the three different types of registration tools (SPM12, DARTEL and ANTs) when a)8mm FWHM, b)10mm FWHM, c)12mm FWHM, d)14mm FWHM, e)16mm FWHM and f)20 mm FWHM smoothing was applied. There are no error bars, because there is a single observation per data point. Label abbreviations: ISC-intersubject correlation; ANTs- Advanced Normalization Tools; SPM- Statistical Parametric Mapping; DARTEL- Diffeomorphic Anatomical Registration Through Exponentiated Lie Algebra.

yielded higher proportions of voxels exhibiting these high correlation values, particularly in the “community” group.

In the “junior ” group, the highest magnitude of the correlation value(r) was 0.67, seen in the data warped by ANTs toolbox at 12mm FWHM smoothing. Likewise, in the“community” data the largest magnitude of the correlation value, although smaller than the “junior” group (0.62) was seen in the data warped by ANTs toolbox at 12mm FWHM smoothing.

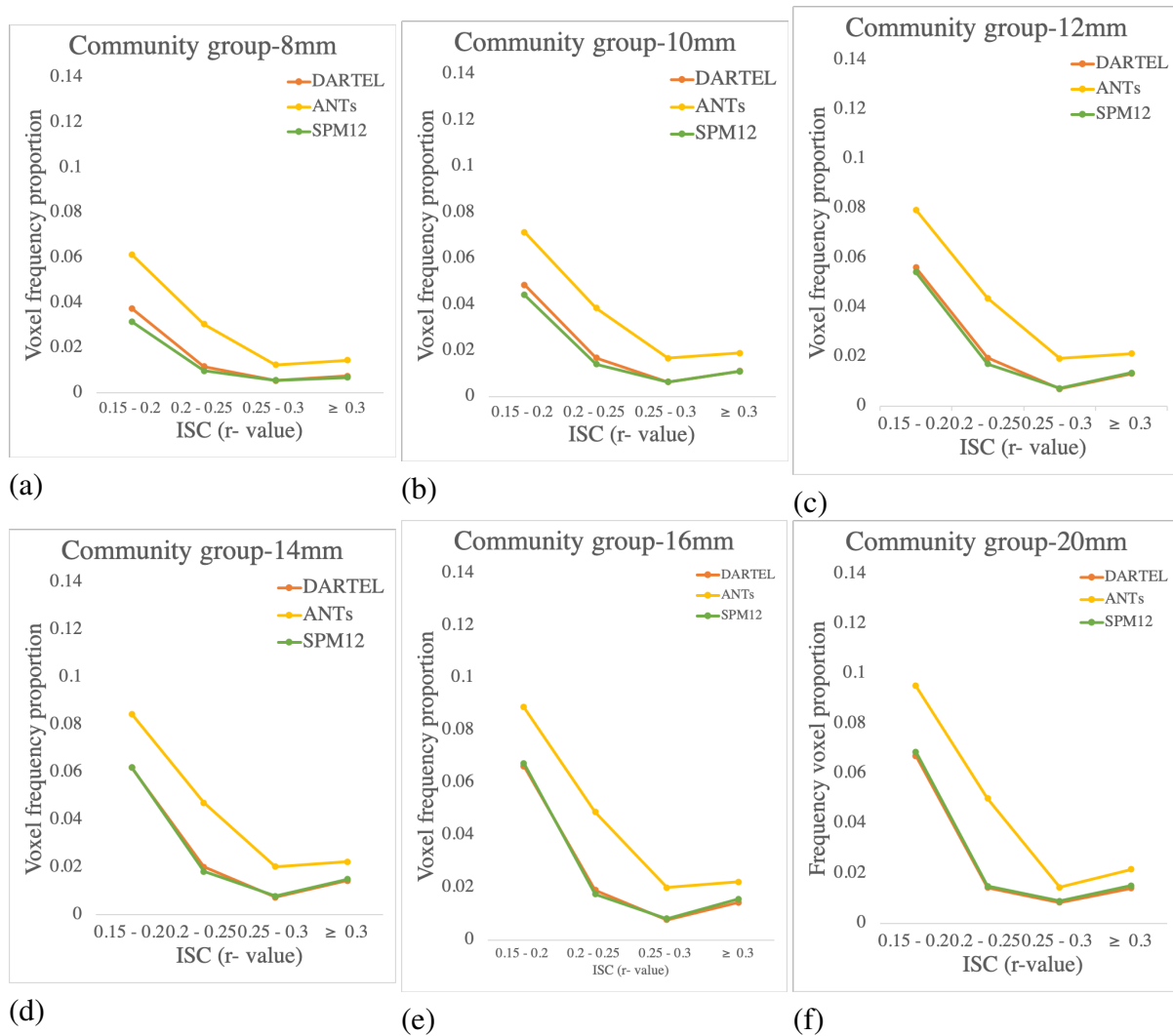


Figure 3.4: Proportion of brain exhibiting ISC higher than the threshold in the “community” group for the three different types of registration tools (SPM12, DARTEL and ANTs) when a)8mm FWHM, b)10mm FWHM, c)12mm FWHM, d)14mm FWHM, e)16mm FWHM and f)20 mm FWHM smoothing was applied. ANTs yielded a higher proportion of voxels with correlation values over 0.15 at all smoothing levels. There are no error bars, because there is a single observation per data point. Label abbreviations: ISC-intersubject correlation; ANTs-Advanced Normalization Tools; SPM- Statistical Parametric Mapping; DARTEL- Diffeomorphic Anatomical Registration Through Exponentiated Lie Algebra.

3.3 Evaluating the pattern of intersubject correlation

To evaluate the pattern of the intersubject correlation across the brain, we compared the mean correlation maps, warped using the three different volume-based normalization methods: ANTs, SPM12, and DARTEL. The images were thresholded at $r = 0.15$, using visu-GUI of the ISC toolbox [16]. Consistent with previous literature [17] [1] [61], the voxel-wise correlation maps

of our study demonstrated widespread, synchronous, hemodynamic cortical activity [1] (Figures 3.5 and 3.6).

The pattern of the distribution of the hemodynamic signal activity was consistent among all three types of software, and the same in the “junior” group and the “community” group. Correlation clusters were significant in temporal, occipital, parietal, and frontal lobes (Figures 3.5 and 3.6). The correlation values were high (between 0.45 and 0.67) in the superior and middle temporal region bilaterally similar to previous works [1] [62].

The maximum correlations (peaks) were consistently located in the superior temporal gyrus bilaterally across all three normalization toolboxes, possibly reflecting responses to the soundtrack of the movie, (Figures 3.5 and 3.6). Besides the superior temporal gyrus, including planum temporale (Wernicke's area) and auditory cortex (Heschl's gyri), the areas with high ISC in the temporal lobe covered most of the anterior temporal pole, medial temporal gyrus and inferior temporo-occipital cortex and temporoparietal junction bilaterally.

In the occipital lobe, we saw high correlation values in medial and lateral visual areas, lingual gyrus, cuneus and precuneus. In the parietal lobe, we detected suprathreshold ISC values across all parietal lobe including, postcentral gyrus, superior and inferior parietal lobules, angular gyrus, and supramarginal gyrus.

In the prefrontal region, the correlation values were lower than other areas (between 0.05 -0.14), and they were lower than the average of 0.24 that was reported in previous work [1]. Correlation values were suprathreshold in lateral areas of the frontal pole bilaterally, right superior frontal gyrus, medial side of the precentral gyrus in frontoparietal regions (more in the right frontal cortex than the left frontal cortex).

Figure 3.5 represents a sample of the correlation at 12mm FWHM smoothing. The 12mm FWHM was chosen because the highest correlation values were detected at this filtering level (Appendix A-C). Figure 3.6 represents different sagittal, axial and coronal sections of the brain, demonstrating widespread cortical synchronous brain activity in different coordinates when data were warped with the ANTs toolbox and smoothed at 12mm FWHM. Colored regions demonstrate the location of areas in which the mean correlation values exceeded the threshold ($r = 0.15$).

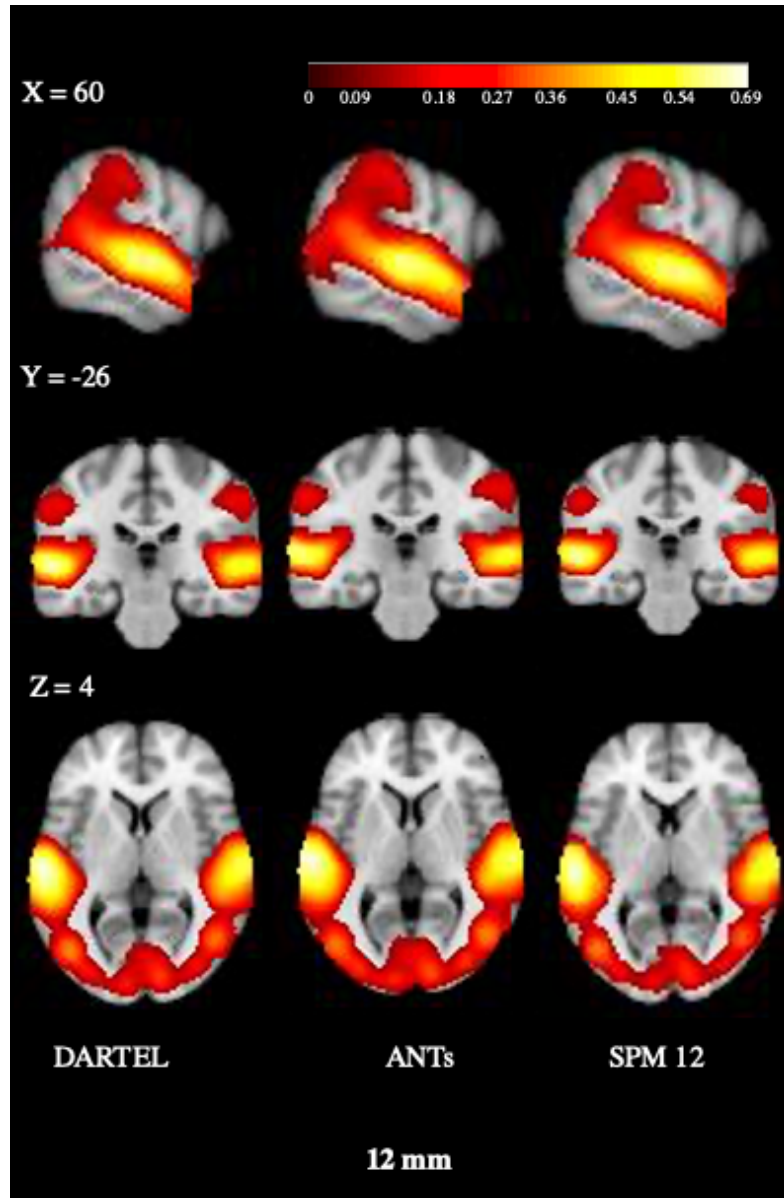


Figure 3.5: Three cross-sections of the mean ISC values generated using three different registration techniques (ANTs, SPM12 and DARTEL) shown at $x=60$, $y=-26$, and $z=4$ in the MNI coordinate frame when 12mm kernel of smoothing was applied. Data are thresholded at a correlation value of $r = 0.15$. The left column corresponds to mean ISC values generated when data were normalized using DARTEL toolbox, the middle column demonstrates ANTs warped data and the right column demonstrates SPM12 warped data. As is shown, the region of highest correlation is around the superior temporal gyrus, bilaterally in all cross-sections. Label abbreviations: ANTs- Advanced Normalization Tools; SPM- Statistical Parametric Mapping; DARTEL- Diffeomorphic Anatomical Registration Through Exponentiated Lie Algebra

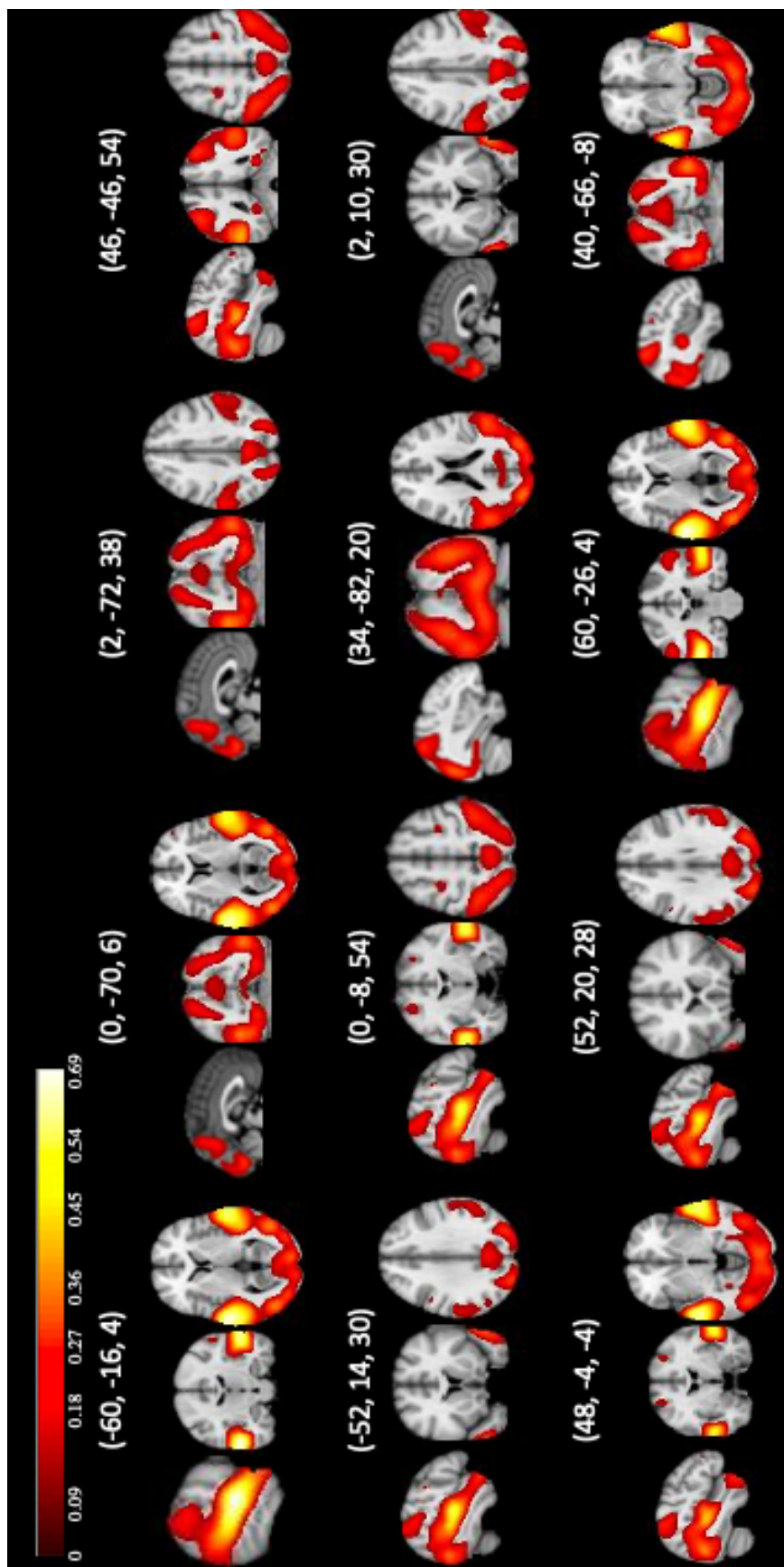


Figure 3.6: Three cross-sections of the mean ISC values generated using ANTs registration techniques shown at different MNI coordinate frames when 12mm kernel of smoothing was applied. Data are thresholded at a correlation value of $r = 0.15$.

3.4 Investigating the similarity in patterns of correlation across normalization methods

In order to compare the spatial similarity of correlation maps from the three types of normalization (separately for each degree of smoothing), I calculated Dice Similarity Coefficients (DSC) pairwise on binarized mean ISC maps. I binarized the correlation maps at an r -value of 0.15 using the ImCalc module of SPM12, turning all values over 0.15 to “1”, and zeroing all other values. The MATLAB version 2019b script, (<http://mathworks.com>) was used for calculating the DSC indices [63] to compare between SPM12 and DARTEL, DARTEL and ANTs, and SPM12 and ANTs, at smoothing kernels of 8, 10, 12, 14, 16 and 20 mm FWHM.

In general, the ISC maps across all three types of normalization were highly similar, with most of DSC indices in “almost perfect agreement”(defined as between 0.81 and 1.00 by Landis and Koch [59]). This pattern was evident in both subgroups, suggesting that the results were reliable (Table 3.2). In the “community” group the DSC indices were slightly weaker, compared to the DSC indices of the “junior” group but were still in the category of “almost perfect agreement”(Table 3.2).

As smoothing increased, so did the similarity between correlation maps in both “junior” and “community” samples. These results suggest that the three normalizations operate quite similarly, although ANTs, and then DARTEL, seem to yield the strongest similarity, consistent with them being the most nonlinear, with the smoothly nonlinear SPM12 yielding consistently less similar patterns (Table 3.2), in both the “junior” and the “community” samples.

	Smoothing (FWHM)	ANTs-DARTEL	ANTs-SPM12	DARTEL-SPM12
Whole data	8mm	0.98	0.95	0.97
	10mm	0.98	0.96	0.98
	12mm	0.99	0.96	0.98
	14mm	0.99	0.97	0.98
	16mm	0.99	0.97	0.98
	20 mm	0.99	0.97	0.98
Junior group	8mm	0.98	0.97	0.98
	10mm	0.99	0.98	0.98
	12mm	0.99	0.98	0.99
	14mm	0.99	0.98	0.99
	16mm	0.99	0.99	0.99
	20mm	0.99	0.99	0.99
Community group	8mm	0.97	0.95	0.97
	10mm	0.98	0.96	0.97
	12mm	0.98	0.97	0.97
	14mm	0.98	0.97	0.98
	16mm	0.99	0.98	0.97
	20 mm	0.99	0.98	0.98

Table 3.2: The Dice Similarity Coefficient for the binarized ISC maps, SPM12-ANTs, SPM12-DARTEL and ANTs-DARTEL at kernels of 8, 10, 12, 14, 16 and 20 mm FWHM of smoothing. The largest similarity index is between ANTs and DARTEL (higher than between ANTs and SPM12, and SPM12 and DARTEL) at 20 mm FWHM smoothing, for the “junior” group, and this pattern is evident in the “community”, suggesting that the results are reliable. Label abbreviations: ISC-intersubject correlation; ANTs- Advanced Normalization Tools; SPM-Statistical Parametric Mapping; DARTEL- Diffeomorphic Anatomical Registration Through Exponentiated Lie Algebra.

Chapter 4

Discussion

4.1 Discussion and conclusion

In this study, we investigate the degree to which various volumetric normalization methods achieve overlap across subjects when preprocessing fMRI data from a naturalistic movie-driven protocol. We use intersubject correlation (ISC), a robust phenomenon observed when different individuals watch the same engaging movie, to quantify functional overlap. The ISC is our dependent variable. Since ISC indicates consistency across individuals (manifesting as higher correlation values), we can use it to measure the degree to which 3 types of nonlinear volumetric normalization achieve functional overlap across people. In addition, because we want to maximize sensitivity for future clinical use, we also evaluated ISC across several different levels of smoothing.

To our knowledge, this is the first application of intersubject correlation in movie-driven fMRI to evaluate registration algorithms and levels of smoothing. We sought to identify the normalization algorithm that yields maximal functional overlap across individuals. Stronger ISC values will enable enhanced sensitivity to abnormality, when comparing activity evoked by the movie-fMRI paradigm in individuals with suspected brain damage, compared to a group of healthy controls. Higher ISC values mean more synchronous brain cortical activity and less variability across normal participants. Reduced variability in a normal sample renders abnormalities in those with neurological abnormalities easier to detect.

We compared three different volumetric registration methods: ANTs, DARTEL and SPM12. At the time we did not have a way to compute ISC on surfaces, and so I was not able to compare these volumetric registrations with a surface-based registration method such as Freesurfer. (see Limitations, below).

In addition, we investigated the effect of six levels of spatial smoothing. Spatial smoothing increases functional overlap, but reduces spatial resolution, so finding the minimum degree of spatial smoothing that produces asymptotically high effect sizes was desired. I aimed to identify the normalization method and smoothing combination that yields maximum overlap (most widespread high intersubject correlation values) with the lowest degree of smoothing. Using this processing strategy will help us to maximize the sensitivity of clinical tests using movie-driven fMRI in the future.

The movie-fMRI paradigm is a non-invasive, reliable and fast method to acquire brain data relevant to cortical organization of function [62] [17]. Watching a movie was a pleasant experience for participants and took less than 10 minutes. Patterns of intersubject correlations were reliable across normalization methods and quite reliable across the smoothing filter widths typically used for fMRI data (8-12mm), and were consistent across two subgroups of our participants' data.

We compared the ISC values of different conditions by assessing the voxel-wise frequency of higher ISC values (r) and by using the Dice Similarity Coefficient (DSC), which is a measure of spatial overlap between two images (in this case, thresholded maps of intersubject correlation). Our results demonstrated that the dimensionality of the normalization toolbox (number of degrees of freedom) and the size of the smoothing kernel directly influenced the magnitude and extent of obtained ISC.

Reviewing the ISC maps results of all 18 different conditions (three types of registration method, six kernels of spatial smoothing for each toolbox) revealed that the pattern of cortical areas in which ISC was detected across the whole brain was similar compared to previous studies using the same movie [17] [1] [61] and other movies [64] [60]. The correlation clusters covered most of the temporal and occipital lobes bilaterally. The parietal and frontal lobes showed synchronous, although weaker compared to temporal and occipital lobes, cortical activity across participants as well, in keeping with previous literature [60] [1] [17].

Most of the DSC indices were in the “almost perfect agreement” category of Landis and Koch [59] (0.8- 1) demonstrating that the spatial patterns of ISC were quite similar across all three normalizations. The patterns were most similar between ANTs and DARTEL, with SPM12 yielding reliably less similar patterns (but only modestly) compared to the other two normalization methods.

We may not have observed as much ISC in frontal regions as previous studies for a couple of reasons. In [17], independent components analysis (ICA) was used for the evaluation of synchronous brain cortical activity, not ISC. Although strong synchronization was reported in the prefrontal areas, the numbers were not statistically comparable to our study, because the

analysis method was different. In our study, the average mean intersubject correlation value (almost 0.09) in frontal lobe was less than the correlation value in similar studies (0.24 in [62]). Comparing the study conducted by Hasson et al. [62] with our study, the following differences were noted: 1) a smaller sample size: while in [62] study the ISC was calculated based on the BOLD signal activity of 8 participants, in our study the number of participants were 44, more than five times of their sample size. More extreme values are possible when sample sizes are small. 2) a different process of calculating the ISC: in [62] they divided the subjects into two groups, “averaged the response time courses in each group, then computed the correlation coefficients between the two resulting response time courses at each cortical location” [62]. In our study, however, for each voxel, the individual's Pearson's correlation coefficient of the fMRI time series was calculated pairwise, and then these were averaged. Averaging the time course responses before calculation of correlation may have enhanced the resulting correlation coefficients. Either or both of these differences may explain the higher correlation value observed in the frontal region in previous work using this movie [62] compared to mine.

Reviewing the voxel-wise ISC frequencies demonstrated that high dimensional volumetric registration algorithms such as ANTs and DARTEL yielded larger ISC values, indicating stronger correspondence across neurologically normal participants. Spatial normalization of fMRI data with these algorithms reduced inter-subject variability in structure, and also in function, relative to the lower dimensional but commonly used algorithm, SPM12. Our study indicates that although SPM12, is popular, it may not be the best choice for normalization of movie-driven fMRI data for mapping of cortical brain function [37]. Furthermore, using a different functional metric (ISC instead of resting state connectivity or activation cluster significance) we have observed that higher-dimensional normalization of structural data enhances overlap of coregistered functional data [23] [22] [24].

The magnitude of the intersubject correlation is a measure of overlap across individuals. In any particular brain area with higher ISC value (r), compared to the areas with lower ISC, we have more functional consistency across individuals at that brain location. By evaluating different kernels of spatial smoothing, keeping an eye on the magnitude of the ISC values as well as the extent, we verified that applying a Gaussian filter of 12 mm FWHM on movie-driven fMRI data resulted in the highest correlation values between participants across the brain [21]. A Gaussian kernel of 12 mm FWHM consistently outperformed smaller filter widths for detection of high ISC values. This degree of spatial smoothing was in agreement with previous work [21] demonstrating that at the filter of 12mm FWHM, the degree of ISC index was the highest. Regarding the total number of detected voxels with a suprathreshold ISC value, the 12mm FWHM was consistently the start of an asymptote for the highest proportion of detected significant voxels across all normalization methods.

Given that the registration algorithms with higher degrees of freedom yielded stronger anatomical overlap across individuals, a gaussian filter of 12mm FWHM (with a voxel size of 3mm) may sound unnecessarily high. While high anatomical alignment across subjects

yields strong functional overlap in primary sensory/ motor areas [24], such alignment yields less (and perhaps no) benefit in higher-order, association, cortices [24]. It is not clear how to compensate for normal, albeit marked, variations in the macroanatomical structure of cortex across individuals. For example, in the case of Heschl’s gyrus mentioned in the introduction, should the normalization squeeze all three gyri in one person to match the single gyrus of another person, or should only the anteriormost gyrus of the two individuals be aligned, with more posterior transverse temporal gyri of Heschl normalized with the planum temporale?. It is not currently clear what method would yield the best functional overlap. Higher smoothing allows us to overcome such residual variability in anatomy, even after high-dimensional normalization.

To assess the generalizability and replicability of our results, we conducted the voxelwise ISC analysis on two independent sets of data: the “community” group and the “junior” group. Both the proportion of brain voxels exhibiting robust synchronous hemodynamic activity, and the spatial patterns of this intersubject correlation as indicated by the DSC measures, were consistent across those groups, which showed the consistency of the results and reproducibility of the method.

4.2 Limitations

The age range of participants in our samples was wide, and differed between the “junior” data and “community” groups. This might be the reason for the differences observed between the results in the “junior” data and “community” samples. Because the correlation in movie-fMRI paradigms is dependent on the participant’s perception and comprehension of the contents of the movie, future studies of this kind would benefit from categorizing the subjects according to demographic and some social criteria, including, but not limited to, age, educational background and ethnicity.

My analysis was largely qualitative, and reliability was assessed by comparing results across independent samples. Although the results were reliable across participant groups, it would be useful in future to quantify, and test, whether ANTs normalization with 12 mm of smoothing provides a statistically significant improvement in the magnitude of ISC, or the extent of clusters exhibiting ISC, relative to other normalization methods and smoothing levels.

In terms of software and computational limitations, we encountered frequent incompatibilities between different image processing toolboxes, analysis software packages, and visualization tools. Investigating the ISC maps with image viewers other than the “visu-GUI” of the ISC toolbox [16] was not technically possible. The functionality of the ISC toolbox was limited. As a result, determining the exact correlation value of single coordinates was not possible.

Additionally, because of multiple factors including, but not limited to, the total number of volumes per subject, the small size of voxels and the high number of iterations (100 million) [28] in calculation of the ISCs, the correlation coefficient matrices were very large and running the MATLAB based analyses required a powerful computational system. In order to smoothly run the analyses and have a systematic system and memory backup, we used a large random access-memory (RAM)(62 GB) desktop computer with a large disk memory that was gradually increased to 8 TB.

4.3 Future directions

The combination of processing steps identified here as optimal will be employed in the next stage of the project (not included in this thesis) in which ISCs of individual patients with temporal lobe epilepsy will be compared to the ISC in a group of demographically matched healthy participants.

Although we show that high-dimensional volumetric normalizations like DARTEL and ANTs are better than another common normalization tool – SPM12 – they may not be as sensitive as surface-based registration algorithms such as FreeSurfer [54], which may provide more precise intersubject registration [65]. It would also be interesting to compare our results other commonly used volumetric registration toolboxes like FSL [66].

Giving the diversity of the age and gender of the participants, particularly in the “community” sample, which was collected to match the demographic characteristics of presurgical candidates with epilepsy, the pattern of cortical brain activity in this group can serve as a normative sample to evaluate the normality of whole-brain dynamic activity in demographically matched patients with neurologic disorders, as they watch the same movie.

The movie-driven fMRI paradigm is advantageous in that it reflects realistic cognitive functions, in normal individuals and those with neurologic disorders. Given the possibility of functional reorganization in patients, a paradigm that maps cognitive functional efficiently, such as a naturalistic movie paradigm, may be helpful. For example, the time series of activity in a given cluster in an individual patient can be compared to time series (via correlation) across various clusters in a normative sample, in order to identify how functionally similar activity is organized in a patient relative to the neurologically normal brain, thus providing a window on functional plasticity. This paradigm may be a strong and reliable adjunct method in presurgical and intraoperative cognitive assessment, potentially leading to better treatment and improved outcomes.

Bibliography

- [1] U. Hasson, O. Landesman, B. Knappmeyer, I. Vallines, N. Rubin, and D. J. Heeger, “Neurocinematics: The Neuroscience of Film,” *Projections*, vol. 2, no. 1, pp. 1–26, 2008.
- [2] J. S. Duncan, G. P. Winston, M. J. Koepp, and S. Ourselin, “Brain imaging in the assessment for epilepsy surgery,” *The Lancet Neurology*, vol. 15, no. 4, pp. 420–433, 2016.
- [3] J. Zhang, W. Liu, H. Chen, H. Xia, Z. Zhou, S. Mei, Q. Liu, and Y. Li, “Multimodal neuroimaging in presurgical evaluation of drug-resistant epilepsy,” *NeuroImage: Clinical*, vol. 4, pp. 35–44, 2014.
- [4] J. J. Falco-Walter, I. E. Scheffer, and R. S. Fisher, “The new definition and classification of seizures and epilepsy,” *Epilepsy Research*, vol. 139, no. November 2017, pp. 73–79, 2018.
- [5] P. Kwan, A. Arzimanoglou, A. T. Berg, M. J. Brodie, W. A. Hauser, G. Mathern, S. L. Moshé, E. Perucca, S. Wiebe, and J. French, “Definition of drug resistant epilepsy: Consensus proposal by the ad hoc Task Force of the ILAE Commission on Therapeutic Strategies,” *Epilepsia*, vol. 51, no. 6, pp. 1069–1077, 2010.
- [6] J. W. Miller and S. Hakimian, “Surgical treatment of epilepsy,” *CONTINUUM Lifelong Learning in Neurology*, vol. 19, no. 3, pp. 730–742, 2013.
- [7] W. L. Ramey, N. L. Martirosyan, C. M. Lieu, H. A. Hasham, G. M. Lemole, and M. E. Weinand, “Current management and surgical outcomes of medically intractable epilepsy,” *Clinical Neurology and Neurosurgery*, vol. 115, no. 12, pp. 2411–2418, 2013.
- [8] K. J. J.T., S. M.R., J. A.C., and O. M.J., “A cost-effectiveness analysis of anterior temporal lobectomy for intractable temporal lobe epilepsy,” *Journal of Neurosurgery*, vol. 87, no. 1, pp. 20–28, 1997.
- [9] C. F. Benjamin, I. Dhingra, A. X. Li, H. Blumenfeld, R. Alkawadri, S. Bickel, C. Helmstaedter, S. Meletti, R. A. Bronen, S. K. Warfield, J. M. Peters, D. Reutens, M. M. Połczyńska, L. J. Hirsch, and D. D. Spencer, “Presurgical language fMRI: Technical practices in epilepsy surgical planning,” *Human Brain Mapping*, vol. 39, no. 10, pp. 4032–4042, 2018.

- [10] A. Schulze-Bonhage and J. Zentner, "The Preoperative Evaluation and Surgical Treatment of Epilepsy," *Deutsches Arzteblatt International*, vol. 111, no. 18, pp. 313–320, 2014.
- [11] S. Baxendale, "The Wada test," *Current Opinion in Neurology*, vol. 22, no. 2, pp. 185–189, 2009.
- [12] L. Caciagli, B. C. Bernhardt, S. J. Hong, A. Bernasconi, and N. Bernasconi, "Functional network alterations and their structural substrate in drug-resistant epilepsy," *Frontiers in Neuroscience*, vol. 8, no. DEC, pp. 1–12, 2014.
- [13] S. Ogawa, T. M. Lee, A. R. Kay, and D. W. Tank, "Brain magnetic resonance imaging with contrast dependent on blood oxygenation," *Proceedings of the National Academy of Sciences of the United States of America*, vol. 87, no. 24, pp. 9868–9872, 1990.
- [14] M. A. Silva, A. P. See, W. I. Essayed, A. J. Golby, and Y. Tie, "Challenges and techniques for presurgical brain mapping with functional MRI," *NeuroImage: Clinical*, vol. 17, no. November 2017, pp. 794–803, 2018.
- [15] U. Hasson, Y. Nir, I. Levy, G. Fuhrmann, and R. Malach, "Intersubject Synchronization of Cortical Activity During Natural Vision," vol. 303, no. MARCH, pp. 1634–1640, 2004.
- [16] J. P. Kauppi, J. Pajula, and J. Tohka, "A versatile software package for inter-subject correlation based analyses of fMRI," *Frontiers in Neuroinformatics*, vol. 8, no. JAN, pp. 1–13, 2014.
- [17] L. Naci, R. Cusack, M. Anello, and A. M. Owen, "A common neural code for similar conscious experiences in different individuals," *Proceedings of the National Academy of Sciences of the United States of America*, vol. 111, no. 39, pp. 14277–14282, 2014.
- [18] M. J. Hamberger and J. Cole, "Language organization and reorganization in epilepsy," *Neuropsychology Review*, vol. 21, no. 3, pp. 240–251, 2011.
- [19] M. Brett, W. Penny, and S. Kiebel, "Introduction to Random Field Theory," *Human Brain Function: Second Edition*, pp. 867–879, 2003.
- [20] C. Warrier, P. Wong, V. Penhune, R. Zatorre, T. Parrish, D. Abrams, and N. Kraus, "Behavioral/Systems/Cognitive Relating Structure to Function: Heschl's Gyrus and Acoustic Processing," 2009.
- [21] J. Pajula and J. Tohka, "Effects of spatial smoothing on inter-subject correlation based analysis of FMRI," *Magnetic Resonance Imaging*, vol. 32, no. 9, pp. 1114–1124, 2014.
- [22] M. A. Frost and R. Goebel, "Measuring structural-functional correspondence: Spatial variability of specialised brain regions after macro-anatomical alignment," *NeuroImage*, vol. 59, no. 2, pp. 1369–1381, 2012.
- [23] M. A. Frost, F. Esposito, and R. Goebel, "Improved correspondence of resting-state networks after macroanatomical alignment," *Human Brain Mapping*, vol. 35, pp. 673–682, feb 2014.

- [24] A. M. Tahmasebi, M. H. Davis, C. J. Wild, J. M. Rodd, H. Hakyemez, P. Abolmaesumi, and I. S. Johnsrude, "Is the link between anatomical structure and function equally strong at all cognitive levels of processing?," *Cerebral Cortex*, vol. 22, no. 7, pp. 1593–1603, 2012.
- [25] J. Crinion, J. Ashburner, A. Leff, M. Brett, C. Price, and K. Friston, "Spatial normalization of lesioned brains: Performance evaluation and impact on fMRI analyses," *NeuroImage*, vol. 37, no. 3, pp. 866–875, 2007.
- [26] M. Mikl, R. Mareček, P. Hlušík, M. Pavlicová, A. Drastich, P. Chlebus, M. Brázdil, and P. Krupa, "Effects of spatial smoothing on fMRI group inferences," *Magnetic Resonance Imaging*, vol. 26, no. 4, pp. 490–503, 2008.
- [27] K. J. Worsley, S. Marrett, P. Neelin, and A. C. Evans, "Searching scale space for activation in PET images," *Human Brain Mapping*, vol. 4, no. 1, pp. 74–90, 1996.
- [28] J. Pajula, *Inter-Subject Correlation Analysis for Functional Magnetic Resonance Imaging: Properties and Validation*. Thesis, Tampere University of Technology, 2016.
- [29] A. M. Tahmasebi, P. Abolmaesumi, Z. Z. Zheng, K. G. Munhall, and I. S. Johnsrude, "Reducing inter-subject anatomical variation: Effect of normalization method on sensitivity of functional magnetic resonance imaging data analysis in auditory cortex and the superior temporal region," *NeuroImage*, vol. 47, no. 4, pp. 1522–1531, 2009.
- [30] J. Ashburner, "SPM: A history," *NeuroImage*, vol. 62, no. 2, pp. 791–800, 2012.
- [31] J. Ashburner, "A fast diffeomorphic image registration algorithm," *NeuroImage*, vol. 38, no. 1, pp. 95–113, 2007.
- [32] B. B. Avants, N. J. Tustison, M. Stauffer, G. Song, B. Wu, and J. C. Gee, "The Insight ToolKit image registration framework," *Frontiers in Neuroinformatics*, vol. 8, no. APR, pp. 1–13, 2014.
- [33] S. A. Huettel, A. W. Song, and G. McCarthy, *Functional Magnetic Resonance Imaging*. Sunderland, MA: Sinauer Associates, INC, 2 ed., 1973.
- [34] A. A. Joshi, *Registration*, pp. 3–12. New York, NY: Springer New York, 2018.
- [35] S. S. Ghosh, S. Kakunoori, J. Augustinack, A. Nieto-castanon, N. Gaab, J. A. Christodoulou, C. Triantafyllou, and D. E. John, "Evaluating the Validity of Volume-Based and Surface-Based Brain Image Registration for Developmental Cognitive Neuroscience Studies in Children 4-to-11 Years of Age," vol. 53, no. 1, pp. 85–93, 2011.
- [36] M. McGill Centre for Integrative Neuroscience, "Atlases," 2020.
- [37] A. Klein, J. Andersson, B. A. Ardekani, J. Ashburner, B. Avants, M. C. Chiang, G. E. Christensen, D. L. Collins, J. Gee, P. Hellier, J. H. Song, M. Jenkinson, C. Lepage, D. Rueckert, P. Thompson, T. Vercauteren, R. P. Woods, J. J. Mann, and R. V. Parsey, "Evaluation of 14 nonlinear deformation algorithms applied to human brain MRI registration," *NeuroImage*, vol. 46, no. 3, pp. 786–802, 2009.

- [38] A. M. Tahmasebi, P. Abolmaesumi, C. Wild, and I. S. Johnsrude, “A validation framework for probabilistic maps using Heschl’s gyrus as a model,” *NeuroImage*, vol. 50, no. 2, pp. 532–544, 2010.
- [39] M. Jenkinson, C. F. Beckmann, T. E. J. Behrens, M. W. Woolrich, and S. M. Smith, “Review FSL,” *NeuroImage*, vol. 62, pp. 782–790, 2012.
- [40] M. Brett, I. S. Johnsrude, and A. M. Owen, “The problem of functional localization in the human brain,” *Nature Reviews Neuroscience*, vol. 3, no. 3, pp. 243–249, 2002.
- [41] F. Crivello, T. Schormann, N. Tzourio-Mazoyer, P. E. Roland, K. Zilles, and B. M. Mazoyer, “Comparison of spatial normalization procedures and their impact on functional maps,” *Human Brain Mapping*, vol. 16, no. 4, pp. 228–250, 2002.
- [42] J. Ashburner and K. J. Friston, “Using Basis Functions,” *Human Brain Mapping*, vol. 266, pp. 254–266, 1999.
- [43] J. Ashburner and T. W. Trust, “SPM12_Manual,” 2020.
- [44] B. B. Avants, N. J. Tustison, G. Song, P. A. Cook, A. Klein, and J. C. Gee, “A reproducible evaluation of ANTs similarity metric performance in brain image registration,” *NeuroImage*, vol. 54, no. 3, pp. 2033–2044, 2011.
- [45] O. Esteban, R. Ciric, K. Finc, R. W. Blair, C. J. Markiewicz, C. A. Moodie, J. D. Kent, M. Goncalves, E. DuPre, D. E. Gomez, Z. Ye, T. Salo, R. Valabregue, I. K. Amlien, F. Liem, N. Jacoby, H. Stojić, M. Cieslak, S. Urchs, Y. O. Halchenko, S. S. Ghosh, A. De La Vega, T. Yarkoni, J. Wright, W. H. Thompson, R. A. Poldrack, and K. J. Gorgolewski, “Analysis of task-based functional MRI data preprocessed with fMRIPrep,” *Nature Protocols*, pp. 1–21, 2020.
- [46] J. Pajula, J. P. Kauppi, and J. Tohka, “Inter-subject correlation in fMRI: Method validation against stimulus-model based analysis,” *PLoS ONE*, vol. 7, no. 8, 2012.
- [47] J. Chen, C. J. Honey, E. Simony, M. J. Arcaro, K. A. Norman, and U. Hasson, “Accessing Real-Life Episodic Information from Minutes versus Hours Earlier Modulates Hippocampal and High-Order Cortical Dynamics,” *Cerebral Cortex*, vol. 26, no. 8, pp. 3428–3441, 2016.
- [48] P. L. Kent, “Evolution of Wechsler’s Memory Scales: Content and structural analysis,” *Applied Neuropsychology:Adult*, vol. 24, no. 3, pp. 232–251, 2017.
- [49] S. A. Nastase, V. Gazzola, U. Hasson, and C. Keysers, “Measuring shared responses across subjects using intersubject correlation,” *Social Cognitive and Affective Neuroscience*, vol. 14, no. 6, pp. 669–687, 2019.
- [50] D. Ladowski, *Using movies to assess cognitive and neural functioning in temporal lobe epilepsy*. PhD thesis, aug 2019.

- [51] K. Gorgolewski, C. D. Burns, C. Madison, D. Clark, Y. O. Halchenko, M. L. Waskom, and S. Ghosh, “Nipype: a flexible, lightweight and extensible neuroimaging data processing framework in Python,” *Frontiers in Neuroinformatics*, vol. 5, p. 13, 2011.
- [52] K. J. Gorgolewski, O. Esteban, C. J. Markiewicz, E. Ziegler, D. G. Ellis, M. P. Notter, D. Jarecka, H. Johnson, C. Burns, A. Manhães-Savio, C. Hamalainen, B. Yvernault, T. Salo, K. Jordan, M. Goncalves, M. Waskom, D. Clark, J. Wong, F. Loney, M. Modat, B. E. Dewey, C. Madison, M. di Oleggio Castello, M. G. Clark, M. Dayan, D. Clark, A. Keshavan, B. Pinsard, A. Gramfort, S. Berleant, D. M. Nielson, S. Bougacha, G. Varoquaux, B. Cipollini, R. Markello, A. Rokem, B. Moloney, Y. O. Halchenko, W. Demian, M. Hanke, C. Horea, J. Kaczmarzyk, G. de Hollander, E. DuPre, A. Gillman, D. Mordom, C. Buchanan, R. Tungaraza, W. M. Pauli, S. Iqbal, S. Sikka, M. Mancini, Y. Schwartz, I. B. Malone, M. Dubois, C. Frohlich, D. Welch, J. Forbes, J. Kent, A. Watanabe, C. Cumba, J. M. Huntenburg, E. Kastman, B. N. Nichols, A. Eshaghi, D. Ginsburg, A. Schaefer, B. Acland, S. Giavasis, J. Kleesiek, D. Erickson, R. Kättner, C. Haselgrove, C. Correa, A. Ghayoor, F. Liem, J. Millman, D. Haehn, J. Lai, D. Zhou, R. Blair, T. Glatard, M. Renfro, S. Liu, A. E. Kahn, F. Pérez-García, W. Triplett, L. Lampe, J. Stadler, X.-Z. Kong, M. Hallquist, A. Chetverikov, J. Salvatore, A. Park, R. Poldrack, R. C. Craddock, S. Inati, O. Hinds, G. Cooper, L. N. Perkins, A. Marina, A. Mattfeld, M. Noel, L. Snoek, K. Matsubara, B. Cheung, S. Rothmei, S. Urchs, J. Durnez, F. Mertz, D. Geisler, A. Floren, S. Gerhard, P. Sharp, M. Molina-Romero, A. Weinstein, W. Broderick, V. Saase, S. K. Andberg, R. Harms, K. Schlamp, J. Arias, D. Papadopoulos Orfanos, C. Tarbert, A. Tambini, A. De La Vega, T. Nickson, M. Brett, M. Falkiewicz, K. Podranski, J. Linkersdörfer, G. Flandin, E. Ort, D. Shachnev, D. McNamee, A. Davison, J. Varada, I. Schwabacher, J. Pellman, M. Perez-Guevara, R. Khanuja, N. Pannetier, C. McDermottroe, and S. Ghosh, “Nipype,” *Software*, 2018.
- [53] V. S. Fonov, A. C. Evans, R. C. McKinstry, C. R. Almli, and D. L. Collins, “Unbiased nonlinear average age-appropriate brain templates from birth to adulthood,” *NeuroImage*, vol. 47, Supple, p. S102, 2009.
- [54] B. Fischl, “FreeSurfer Authos Manuscript,” *NeuroImage*, vol. 62, no. 2, pp. 774–781, 2012.
- [55] R. W. Cox and J. S. Hyde, “Software tools for analysis and visualization of fMRI data,” *NMR in Biomedicine*, vol. 10, no. 4-5, pp. 171–178, 1997.
- [56] J. D. Power, A. Mitra, T. O. Laumann, A. Z. Snyder, B. L. Schlaggar, and S. E. Petersen, “Methods to detect, characterize, and remove motion artifact in resting state fMRI,” *NeuroImage*, vol. 84, no. Supplement C, pp. 320–341, 2014.
- [57] Y. Behzadi, K. Restom, J. Liau, and T. T. Liu, “A component based noise correction method (CompCor) for BOLD and perfusion based fMRI,” *NeuroImage*, vol. 37, no. 1, pp. 90–101, 2007.
- [58] K. H. Zou, S. K. Warfield, A. Bharatha, C. M. Tempany, M. R. Kaus, S. J. Haker, W. M. Wells, F. A. Jolesz, and R. Kikinis, “Statistical Validation of Image Segmentation Quality

- Based on a Spatial Overlap Index,” *Academic Radiology*, vol. 11, no. 2, pp. 178–189, 2004.
- [59] J. R. Landis and G. G. Koch, “The Measurement of Observer Agreement for Categorical Data,” *Biometrics*, vol. 33, no. 1, pp. 159–174, 1977.
- [60] J. P. Kauppi, I. P. Jääskeläinen, M. Sams, and J. Tohka, “Inter-subject correlation of brain hemodynamic responses during watching a movie: Localization in space and frequency,” *Frontiers in Neuroinformatics*, vol. 4, no. MAR, pp. 1–10, 2010.
- [61] K. L. Campbell, M. A. Shafto, P. Wright, K. A. Tsvetanov, L. Geerligs, R. Cusack, L. K. Tyler, C. Brayne, E. Bullmore, A. Calder, T. Dalgleish, J. Duncan, R. Henson, F. Matthews, W. Marslen-Wilson, J. Rowe, T. Cheung, S. Davis, R. Kievit, A. McCarrey, D. Price, J. Taylor, N. Williams, L. Bates, T. Emery, S. Erzinçlioglu, A. Gadie, S. Gerbase, S. Georgieva, C. Hanley, B. Parkin, D. Troy, J. Allen, G. Amery, L. Amunts, A. Barcroft, A. Castle, C. Dias, J. Dowrick, M. Fair, H. Fisher, A. Goulding, A. Grewal, G. Hale, A. Hilton, F. Johnson, P. Johnston, T. Kavanagh-Williamson, M. Kwasniewska, A. McMinn, K. Norman, J. Penrose, F. Roby, D. Rowland, J. Sargeant, M. Squire, B. Stevens, A. Stoddart, C. Stone, T. Thompson, O. Yazlik, M. Dixon, D. Barnes, J. Hillman, J. Mitchell, and L. Willis, “Idiosyncratic responding during movie-watching predicted by age differences in attentional control,” *Neurobiology of Aging*, vol. 36, pp. 3045–3055, nov 2015.
- [62] U. Hasson, R. Malach, and D. J. Heeger, “Reliability of cortical activity during natural stimulation,” *Trends in Cognitive Sciences*, vol. 14, pp. 40–48, jan 2010.
- [63] C. Rorden, “GitHub,” 2020.
- [64] A. Herbec, J. P. Kauppi, C. Jola, J. Tohka, and F. E. Pollick, “Differences in fMRI intersubject correlation while viewing unedited and edited videos of dance performance,” *Cortex*, vol. 71, pp. 341–348, 2015.
- [65] B. Conroy, B. Singer, P. Ramadge, and J. Haxby, “Inter-subject Functional Connectivity Alignment,” in *proceedings from the conference, ”Neural Information Processing Systems 2009.”*, pp. 100–100, proceedings from the conference, ”Neural Information Processing Systems 2009.”, 2009.
- [66] S. M. Smith, M. Jenkinson, M. W. Woolrich, C. F. Beckmann, T. E. Behrens, H. Johansen-Berg, P. R. Bannister, M. De Luca, I. Drobnjak, D. E. Flitney, R. K. Niazy, J. Saunders, J. Vickers, Y. Zhang, N. De Stefano, J. M. Brady, and P. M. Matthews, “Advances in functional and structural MR image analysis and implementation as FSL,” *NeuroImage*, vol. 23, no. SUPPL. 1, pp. 208–219, 2004.

Chapter 5

Appendix

IS(C/R) CONDITION	0- 0.05	0.05-0.1	0.1-0.15	0.15- 0.2	0.2-0.25	0.25- 0.3	0.3-0.35	0.35-0.4	0.4-0.45	0.45-0.5	0.5-0.55	0.55-0.60	0.60-0.65	0.65-0.70
WD8	791548	51854	24731	13354	6673	1960	978	807	547	323	112	0	0	0
WA8	791547	49810	25344	15363	9275	4016	1469	901	668	493	302	106	0	0
WS8	790482	49228	22962	12332	4544	1387	909	700	467	192	56	0	0	0
WD10	778805	57924	28201	15512	8481	2856	1207	925	712	502	208	64	0	0
WA10	779773	55205	27042	17170	11026	5274	2020	1021	793	622	428	214	31	0
WS10	777893	54953	26222	14758	6867	1939	1056	864	642	367	154	23	0	0
WD12	770165	62732	30091	17042	9381	3267	1278	1003	817	577	258	84	0	0
WA12	770346	60529	28143	18236	12335	5975	2300	1149	889	692	499	254	52	0
WS12	768048	59871	28765	16581	8052	2364	1197	934	770	484	181	52	0	0
WD14	763844	66886	31400	18051	10003	3147	1354	1086	869	617	263	63	0	0
WA14	763054	65288	28946	19184	13144	6250	2341	1240	938	758	528	236	29	0
WS14	760852	64233	30388	17788	8675	2522	1312	1009	826	538	198	38	0	0
WD16	759245	70642	32288	18938	10078	2809	1428	1139	907	597	223	20	0	0
WA16	757113	69707	29566	20206	13446	6218	2224	1291	989	788	514	179	1	0
WS16	755390	68346	31634	18752	8798	2372	1395	1087	865	510	196	6	0	0
WD20	753184	76777	34568	20327	8478	2150	1554	1202	868	382	48	0	0	0
WA20	747394	78036	30973	22216	13587	5054	1845	1379	1043	760	290	12	0	0
WS20	747690	75717	34079	20224	7298	2092	1512	1159	830	331	35	0	0	0

Appendix A: Frequency of detected voxels for different normalization and smoothing condition, based on correlation value (r) for whole data ($n=44$). Abbreviations: W- Whole data; A- ANTs toolbox; S- SPM12 toolbox; D- DARTEL toolbox. Numbers correspond to the smoothing kernel in mm FWHM.

CONDITION	0. -> 0.05	0.05 -> 0.1	0.1 -> 0.15	0.15 -> 0.2	0.2 -> 0.25	0.25 -> 0.3	0.3 -> 0.35	0.35 -> 0.4	0.4 -> 0.45	0.45 -> 0.5	0.5 -> 0.55	0.55 -> 0.60	0.60 -> 0.65	0.65 -> 0.70
JD8	768565	53803	29742	18990	11721	6947	3051	1308	828	610	461	283	37	0
JA8	770331	51945	28007	19005	12607	6744	3045	1312	913	585	490	307	65	0
JS8	767800	52483	30225	18087	10910	5480	1996	946	747	517	333	125	25	0
JD10	757086	57117	32197	21668	13425	8525	4020	1688	1055	746	565	438	97	0
JA10	760663	55325	29742	20960	13830	8506	4022	1635	1089	748	572	433	157	2
JS10	756404	55733	32388	20980	13053	7298	2867	1334	887	666	507	230	54	0
JD12	750071	59418	33328	23739	14481	9222	4338	1771	1229	849	642	486	84	0
JA12	753531	58073	31300	22268	14764	9486	4584	1868	1212	854	655	512	147	3
JS12	748413	58651	33552	23240	14505	8253	3382	1536	1057	748	616	281	57	0
JD14	745038	61379	34230	25169	15433	9512	4295	1768	1316	901	713	443	41	0
JA14	747704	61022	32638	23256	15542	9958	4692	1956	1311	946	707	511	106	0
JS14	742423	61518	34547	24806	15626	8775	3423	1654	1144	848	643	284	26	0
JD16	741129	63422	35263	26198	16218	9467	3857	1813	1300	956	716	335	0	0
JA16	742943	63980	33907	24166	16099	10108	4522	1943	1377	975	785	413	50	0
JS16	737489	64575	35529	26019	16442	8980	3138	1718	1189	895	653	197	0	0
JD20	735971	66871	37519	28145	17240	8233	2791	1852	1265	962	520	2	0	0
JA20	734972	70380	35525	25979	16925	9512	3676	1935	1399	1052	663	109	0	0
JS20	730069	69771	38422	27797	17773	7669	2599	1748	1187	921	399	1	0	0

Appendix B: Frequency of detected voxels for different normalization and smoothing condition, based on correlation value (r) for the junior group ($n=22$). Abbreviations: J- Junior group; A- ANT's toolbox; S- SPM12 toolbox; D- DARTEL toolbox. Numbers correspond to the smoothing kernel in mm FWHM.

CONDITION	IS(C/R)															
	0- 0.05	0.05- 0.1	0.1- 0.15	0.15- 0.2	0.2- 0.25	0.25- 0.3	0.3- 0.35	0.35- 0.4	0.4- 0.45	0.45- 0.5	0.5- 0.55	0.55- 0.60	0.60- 0.65	0.65- 0.70		
CD8	794887	56583	20753	8239	2596	1219	828	479	261	95	0	0	0	0		
CA8	778911	60031	25466	13563	6766	2778	1253	814	569	358	174	54	0	0		
CS8	793936	53919	18791	6289	1970	1120	740	424	193	29	0	0	0	0		
CD10	781513	65583	25427	10682	3709	1416	1028	729	399	214	79	0	0	0		
CA10	764223	67335	29248	15769	8488	3700	1567	958	698	497	306	137	15	0		
CS10	780692	62726	23692	8782	2808	1273	1000	682	326	167	21	0	0	0		
CD12	772551	71006	28655	12332	4302	1551	1129	848	507	263	142	2	0	0		
CA12	752217	73462	32692	17536	9653	4253	1677	1025	806	593	374	177	39	0		
CS12	770472	68736	27492	10776	3394	1448	1096	817	487	208	72	0	0	0		
CD14	765810	75070	31329	13651	4434	1628	1214	927	577	288	147	4	0	0		
CA14	743067	78129	36003	18694	10420	4467	1685	1106	872	632	419	179	29	0		
CS14	762914	73066	30461	12355	3611	1565	1169	895	569	245	92	0	0	0		
CD16	760039	78193	34263	14609	4184	1700	1283	950	611	282	22	0	0	0		
CA16	736054	81555	39154	19638	10790	4408	1569	1167	927	654	399	167	4	0		
CS16	756743	76246	33728	13409	3482	1625	1243	951	586	250	76	0	0	0		
CD20	751169	83773	40292	14762	3154	1842	1356	994	525	219	9	0	0	0		
CA20	726460	86406	44649	21024	11066	3189	1644	1281	943	606	277	31	0	0		
CS20	747094	82077	39864	13674	2965	1771	1339	954	511	187	1	0	0	0		

Appendix C: Frequency of detected voxels for different normalization and smoothing condition, based on correlation value (r) for the community group ($n=22$). Abbreviations: C- Community group; A- ANTs toolbox; S- SPM12 toolbox; D- DARTEL toolbox. Numbers correspond to the smoothing kernel in mm FWHM.

Smoothing (mm FWHM)	Normalization	0.15 ≤ r < 0.2	0.2 ≤ r < 0.25	0.25 ≤ r < 0.3	r ≥ 0.3
8	DARTEL	0.06066746	0.030315558	0.008904315	0.01257053
	ANTS	0.070120908	0.042333621	0.018330116	0.01797867
10	SPM12	0.062673748	0.023093538	0.007049018	0.01181104
	DARTEL	0.070471293	0.038529334	0.012974859	0.01643664
12	ANTS	0.078368547	0.050325661	0.024071969	0.02341015
	SPM12	0.075003176	0.034899499	0.009854395	0.01578533
14	DARTEL	0.07742211	0.04261805	0.014842039	0.0182493
	ANTS	0.08323406	0.056300293	0.027271524	0.02663253
16	SPM12	0.084268035	0.040921912	0.012014332	0.01838742
	DARTEL	0.082006015	0.045443807	0.014296877	0.01931691
18	ANTS	0.08756099	0.059992788	0.028526699	0.02770513
	SPM12	0.090402256	0.044088125	0.01281732	0.01992732
20	DARTEL	0.086035672	0.045784534	0.012761337	0.01959858
	ANTS	0.092225676	0.061371199	0.028380642	0.02732173
22	SPM12	0.095301502	0.044713237	0.012054989	0.02062867
	DARTEL	0.092345924	0.038515705	0.009767488	0.01841739
24	ANTS	0.101399862	0.062014761	0.02306783	0.024323
	SPM12	0.102782507	0.03708993	0.010631972	0.01965289

Appendix D: Proportion of voxels exhibiting correlation value (r), above 0.15 for the Whole data. Abbreviations: ANTs- Advanced Normalization Tools; SPM- Statistical Parametric Mapping; DARTEL- Diffeomorphic Anatomical Registration Through Exponentiated Lie Algebra.

Smoothing (mm FWHM)	Normalization	$0.15 \leq r < 0.2$	$0.2 \leq r < 0.25$	$0.25 \leq r < 0.3$	$r \geq 0.3$
8	DARTEL	0.08349418	0.05153424	0.030544185	0.028921786
	ANTS	0.08615141	0.05714869	0.03057117	0.030448776
	SPM 12	0.0853966	0.05151086	0.025873466	0.02213881
10	DARTEL	0.09526866	0.0590263	0.037482248	0.037851575
	ANTS	0.0950136	0.06269266	0.038558477	0.039247507
	SPM12	0.09905571	0.0616289	0.034457035	0.030901794
12	DARTEL	0.10437432	0.06366926	0.040546779	0.041325003
	ANTS	0.10094288	0.06692656	0.043000907	0.044582956
	SPM12	0.10972616	0.06848442	0.038966006	0.036246459
14	DARTEL	0.11066167	0.06785496	0.041821835	0.041667949
	ANTS	0.10542158	0.07045331	0.045140526	0.046368994
	SPM12	0.11711992	0.07377715	0.041430595	0.037875354
16	DARTEL	0.11518592	0.0713064	0.041623982	0.039469577
	ANTS	0.10954669	0.07297824	0.04582049	0.045625567
	SPM12	0.12284703	0.07762984	0.042398489	0.036779981
20	DARTEL	0.12374638	0.07579988	0.036198399	0.032500736
	ANTS	0.11776519	0.07672257	0.043118767	0.040045331
	SPM12	0.13124174	0.08391407	0.036208687	0.032365439

Appendix E: Proportion of voxels exhibiting correlation value (r), above 0.15 for the junior group. Abbreviations: ANTs- Advanced Normalization Tools; SPM- Statistical Parametric Mapping; DARTEL- Diffeomorphic Anatomical Registration Through Exponentiated Lie Algebra; NA- Not applicable.

Smoothing (mm FWHM)	Normalization	0.15 ≤ r < 0.2	0.25 ≤ r < 0.25	0.25 ≤ r < 0.3	r ≥ 0.3
8	DARTEL	0.037429924	0.011793674	0.005537939	0.00755504
	ANTS	0.061353828	0.030606798	0.01256661	0.0145751
	SPM 12	0.031607621	0.00990094	0.005628961	0.00696584
10	DARTEL	0.048528517	0.016850053	0.006432913	0.01112585
	ANTS	0.071332929	0.038396468	0.016737386	0.01889968
	SPM12	0.044137085	0.014112609	0.006397917	0.01103678
12	DARTEL	0.056024496	0.019544063	0.007046221	0.01313386
	ANTS	0.079326162	0.043666483	0.019238947	0.02122029
	SPM12	0.054158646	0.017057762	0.007277442	0.0134693
14	DARTEL	0.062016736	0.020143741	0.007396033	0.01434231
	ANTS	0.084519275	0.047136098	0.020207001	0.02226525
	SPM12	0.062094476	0.018148373	0.007865468	0.0149268
16	DARTEL	0.066368948	0.019007987	0.00772313	0.01430142
	ANTS	0.088834807	0.048809836	0.019940107	0.02210692
	SPM12	0.06739173	0.017500038	0.008167019	0.01561032
20	DARTEL	0.067064029	0.014328678	0.008368239	0.01409698
	ANTS	0.095104541	0.050058355	0.014425817	0.02163194
	SPM12	0.068723583	0.014901669	0.008900795	0.01503737

Appendix F: Proportion of voxels exhibiting correlation value (r), above 0.15 for the community group. Abbreviations:
ANTS- Advanced Normalization Tools; SPM- Statistical Parametric Mapping; DARTEL- Diffeomorphic
Anatomical Registration Through Exponentiated Lie Algebra; NA- Not applicable.



Office of Research Ethics

The University of Western Ontario
Room 4180 Support Services Building, London, ON, Canada N6A 5C1
Telephone: (519) 661-3036 Fax: (519) 850-2466 Email: ethics@uwo.ca
Website: www.uwo.ca/research/ethics

Use of Human Subjects - Ethics Approval Notice

Principal Investigator: Dr. T.M. Peters

Review Number: 16189

Review Level: Full Board

Review Date: May 19, 2009

Protocol Title: Structural and Functional MR imaging in Frontal and Temporal Lobe Epilepsy at 1.5T, 3T, and 7T

Department and Institution: Imaging, Roberts Research Institute

Sponsor: CIHR-CANADIAN INSTITUTE OF HEALTH RESEARCH

Ethics Approval Date: October 7, 2009

Expiry Date: July 31, 2015

Documents Reviewed and Approved: UWO Protocol, Letter of information & consent form dated Aug. 31/09 & Advertisement dated Aug. 31/09

Documents Received for Information:

This is to notify you that The University of Western Ontario Research Ethics Board for Health Sciences Research Involving Human Subjects (HSREB) which is organized and operates according to the Tri-Council Policy Statement: Ethical Conduct of Research Involving Humans and the Health Canada/ICH Good Clinical Practice Practices: Consolidated Guidelines; and the applicable laws and regulations of Ontario has reviewed and granted approval to the above referenced study on the approval date noted above. The membership of this REB also complies with the membership requirements for REB's as defined in Division 5 of the Food and Drug Regulations.

The ethics approval for this study shall remain valid until the expiry date noted above assuming timely and acceptable responses to the HSREB's periodic requests for surveillance and monitoring information. If you require an updated approval notice prior to that time you must request it using the UWO Updated Approval Request Form.

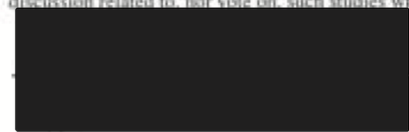
During the course of the research, no deviations from, or changes to, the protocol or consent form may be initiated without prior written approval from the HSREB except when necessary to eliminate immediate hazards to the subject or when the change(s) involve only logistical or administrative aspects of the study (e.g. change of monitor, telephone number). Expedited review of minor change(s) in ongoing studies will be considered. Subjects must receive a copy of the signed information/consent documentation.

Investigators must promptly also report to the HSREB:

- a) changes increasing the risk to the participant(s) and/or affecting significantly the conduct of the study;
- b) all adverse and unexpected experiences or events that are both serious and unexpected;
- c) new information that may adversely affect the safety of the subjects or the conduct of the study.

If these changes/adverse events require a change to the information/consent documentation, and/or recruitment advertisement, the newly revised information/consent documentation, and/or advertisement, must be submitted to this office for approval.

Members of the HSREB who are named as investigators in research studies, or declare a conflict of interest, do not participate in discussion related to, nor vote on, such studies when they are presented to the HSREB.



Chair of HSREB Dr. Joseph Gibert

Ethics Officer to Contact for Further Information

This is an official document. Please retain the original in your files.

cc: GRE File (HR)



**Western University Health Science Research Ethics Board
HSREB Amendment Approval Notice**

Principal Investigator: Dr. Terry Peters

Department & Institution: Schulich School of Medicine and Dentistry/Medical Biophysics, Robarts Research Institute

Review Type: Full Board

HSREB File Number: 6259

Study Title: Structural and Functional MR imaging in Frontal and Temporal Lobe Epilepsy at 1.5T, 3T, and 7T (REB #16189)

Sponsor: Canadian Institutes of Health Research

HSREB Amendment Approval Date: December 21, 2015

HSREB Expiry Date: May 19, 2016

Documents Approved and/or Received for Information:

Document Name	Comments	Version Date
Advertisement	Poster for Control Recruitment	2015/11/18
Advertisement	Recruitment Brochure	2015/11/12
Revised Western University Protocol	Updated Protocol Nov 2015 (Clean)	2015/11/13
Revised Letter of Information & Consent	Volunteers	2015/12/14
Revised Letter of Information & Consent	Patients	2015/12/14
Recruitment Items	Poster-Received Dec 9, 2015	2015/12/09
Instruments	Conditional Associative Learning Test	2015/12/18
Instruments	Doors and People - Sample Doors Item	2015/12/18
Instruments	Doors and People - Sample Names Item	2015/12/18
Instruments	Doors and People Administration Instructions	2015/12/18
Instruments	Matrix Reasoning Record Form	2015/12/18
Instruments	Matrix Reasoning Sample Stimulus Pages	2015/12/18
Instruments	Matrix Reasoning, Vocabulary Administration Instructions	2015/12/18
Instruments	RVDLT Administration Chapter (Spreen 1991)	2015/12/18
Instruments	Vocabular Record Form	2015/12/18
Instruments	Vocabulary Sample Stimulus Page	2015/12/18



Research Ethics

The Western University Health Science Research Ethics Board (HSREB) has reviewed and approved the amendment to the above named study, as of the HSREB Initial Approval Date noted above.

HSREB approval for this study remains valid until the HSREB Expiry Date noted above, conditional to timely submission and acceptance of HSREB Continuing Ethics Review.

The Western University HSREB operates in compliance with the Tri-Council Policy Statement Ethical Conduct for Research Involving Humans (TCPS2), the International Conference on Harmonization of Technical Requirements for Registration of Pharmaceuticals for Human Use Guideline for Good Clinical Practice Practices (ICH E6 R1), the Ontario Personal Health Information Protection Act (PHIPA, 2004), Part 4 of the Natural Health Product Regulations, Health Canada Medical Device Regulations and Part C, Division 5, of the Food and Drug Regulations of Health Canada.

Members of the HSREB who are named as Investigators in research studies do not participate in discussions related to, nor vote on such studies when they are presented to the REB.

The HSREB is registered with the U.S. Department of Health & Human Services under the IRB registration number IRB 00000940.



Ethics Officer, on behalf of Dr. Joseph Gilbert, HSREB Chair

Ethics Officer to Contact for Further Information: Erika Basile ___ Nicole Kanski ___ Grace Kelly ___ Mira Mekhal ___ Viki Tran ___

This is an official document. Please retain the original in your files

Curriculum Vitae

Name	Nargess Ghazaleh
Post-Secondary Education and Degrees	Hamadan University of Medical Science Hamedan, Iran 1998- 2006 M.D. The University of Western Ontario, London, ON 2016 - 2020 (pres) M.Sc.

Publications:

1. Ebrahimi-Rad R, Omrani-Nava M, Molla M, Abdollahpour M, **Ghazaleh N**. Comparison of Antibody Against Chlamydomphila pneumoniae in Patients with Brain Ischemic Stroke. *Advanced Studies in Medical Sciences*. 2014;2: 79-85 (Peer reviewed)
2. Haddadinezhad S, **Ghazaleh N**, Razavi Z. Effect of L-Carnitine on Glycemic Control and C-peptide in Patients with type 2 Diabetes Mellitus. *Turkish Journal of Endocrinology and Metabolism*. 2008; 12(1):1-3(Peer reviewed)
3. **Ghazaleh N**, Haddadinezhad S, Jafari M. Fine Needle Aspiration Cytology of Thyroid Nodules: Correlation with Surgical Histopathology. *Turkish Journal of Endocrinology and Metabolism*. 2008;12(3):73-74(Peer reviewed)
4. Haddadinezhad S, **Ghazaleh N**. Relation of Fasting and Postprandial Plasma Glucose to Glycosylated Hemoglobin in Diabetics patients. *Rawal Medical Journal*. 2008; 33(1): 12-14.(Peer reviewed)
5. Jafari M, **Ghazaleh N**, Haddadinezhad S. FNA as the Best and Cost-Benefit Method in Managing Thyroid Nodules and Comparing the Cytology Results with Pathology Results. In: *Proceeding of the 2nd congress of Iranian Cancer Association, 8th congress of Iranian Society of Pathology*. Tehran, Iran;2006.